

Quantum algorithm for the collision-coalescence of cloud droplets

Kazumasa Ueno^{1,*} and Hiroaki Miura¹

¹*The University of Tokyo*

(Dated: March 9, 2026)

Quantum computing is gaining attention as a new approach for solving complex problems in many scientific fields. In atmospheric and oceanic sciences, it may help reduce computational costs of simulating large and nonlinear systems. However, research into the use of quantum computers in this area is still in its earlier stage, and suitable applications have not been established yet. This study explores the use of quantum computing for calculating the collision-coalescence process of cloud droplets, which dominates the size growth of liquid particles in the cloud microphysics. Inspired by the quantum algorithms developed in the field of financial engineering, we propose a new algorithm based on a master equation that describes the time evolution of the droplet mass distribution. Our algorithm uses the quantum amplitudes to encode the probability distribution of droplet mass and calculates the expected number of droplets via the quantum amplitude estimation. Our resource analysis shows that the number of T gates scales as $\mathcal{O}(N^2)$, where N is the number of bins of the mass distributions. This is an essential improvement over the classical methods that scale only exponentially with N . This efficiency improvement is achieved by using quantum arithmetic in the superposition and by encoding the transition histories instead of the full distributions at each time step. Our results suggest that the collision-coalescence process is one of the promising targets of quantum computing in the field of atmospheric science.

I. INTRODUCTION

Numerical modeling is an essential approach for understanding the atmosphere-ocean system. The key reason is that the system is too complex to be fully understood through analytical methods, and direct experiments of the system are almost impossible. Our understanding of atmospheric and oceanic phenomena has advanced alongside the development of computers. For example, advances in computing have enabled climate-model projections to become more complex, with more detailed representations of physical processes at higher resolution. Despite the inherent limitations of numerical models, these models compute responses of the climate system to the rapid increase of the greenhouse-gas concentrations, and provide useful insights into future climate change [1–5].

It is important to handle stochasticity in these simulations to enhance their realism. This is because the system is nonlinear and chaotic, and thus, even small perturbations can grow into large differences in the future. Stochasticity arises in various ways and can be represented in diverse manners. For example, ensemble simulations are widely used in climate modeling to account for uncertainties arising from initial conditions and intrinsic fluctuations, and to estimate the system's mean behavior [6–8]. Stochastic representations are also used in parameterizations, which are necessary for incorporating interactions between grid-scale (resolved) processes and subgrid-scale (unresolved) processes in numerical models. It is known that incorporating stochastic effects into parameterizations improves representations of the resolved flow, such as the enhanced accuracy of

the mean-state, noise-induced regime transitions, and a more realistic response to external forcing [9]. There are various approaches to incorporating stochastic effects in parameterizations; the super-parameterization method [10, 11], stochastic parameterizations [12–14], and methods based on probability distributions [15–17]. The super-parameterization represents subgrid-scale processes by embedding a reduced-dimension higher-resolution model within the main model. Stochastic parameterizations introduce stochastic perturbations to account for the influence of the unresolved variability. Methods based on probability distributions explicitly consider the probability distributions of the quantities of interest. This third approach has been primarily applied in cloud microphysics.

Cloud microphysics describes the phase change of water in the atmosphere and is one of the most critical processes in atmospheric models. It includes the growth of cloud droplets by the collision-coalescence process. This process is associated with the cloud properties such as droplet size distribution, droplet number concentration, and optical properties. Accurate representations of microphysical processes are essential for numerical models, but achieving them remains a significant challenge. One key reason is the inherent stochasticity of cloud microphysics. Another is that cloud droplets span a wide range of sizes [18].

To address the stochasticity in cloud microphysics, several approaches have been developed; the spectral bin method [15–17], the super-droplet method [19, 20], and the master equation method [21, 22]. Each of these methods is designed to capture different aspects of cloud droplet behaviors, and has its strengths and limitations due to its design. The spectral bin method discretizes droplet size into bins and predicts the time evolution of the droplet size distribution. In this method, the stochas-

* kazumasa-e67@eps.s.u-tokyo.ac.jp

ticity of droplet growth is reflected only through its effect on the ensemble-mean size distribution, so fluctuations of the distribution itself are not explicitly represented. The super-droplet method goes a step further by partially accounting for fluctuations in the droplet size distribution, offering a more detailed representation of variability in the droplet size distribution. The master equation method considers all possible distributions of cloud droplet size, serving as a comprehensive reference for evaluating and refining other parameterization methods. While the master equation method is the closest to the first principles among the three methods, solving the master equation is computationally challenging because the number of possible states grows exponentially with the number of bins. The Monte Carlo method is commonly used to solve the master equation [23], but it still requires a large number of calculations.

In the area of financial engineering, various quantum algorithms have been proposed to solve stochastic differential equations on fault-tolerant quantum computers (FTQCs) [24, 25]. These algorithms are used to calculate the time evolution of financial derivatives and to determine the optimal options for maximizing returns. The underlying assumption is that the variations of derivatives follow master equations. By utilizing the properties of quantum dynamics such as the quantum superposition, interference, and entanglement, the quantum computation can efficiently handle higher-dimensional probability distributions. In addition, the quantum amplitude estimation [26, 27] enables efficient computations of key characteristics derived from these probability distributions, further enhancing the applicability of quantum algorithms in financial modeling.

Here, inspired by the quantum computing in the financial modeling [28], we develop a quantum algorithm to solve the master equation governing the collision-coalescence process of cloud droplets. We can utilize similar principles used in quantum-enhanced financial computations for handling higher-dimensional probability distributions.

Previous quantum algorithms in financial modeling can compute the time evolution of a probability distribution, but they typically focus on a single stochastic variable (e.g., an asset price). In this work, we overcome this limitation by constructing a quantum algorithm that evolves multivariate probability distributions. A straightforward generalization would require a prohibitively large number of qubits to represent all variables explicitly. Instead, we exploit the fact that the number of allowed state transitions is small in the systems considered here. More specifically, we achieve an efficient representation by encoding only the transition types (pathways) rather than the full state history. This efficient handling of multivariate distributions is not only relevant to cloud droplet growth, but also to other stochastic systems with complex interactions such as chemical reaction networks.

This paper is organized as follows. In Sec. II, we summarize the formulation of the cloud collision-coalescence

process based on the master equation in [22]. In Sec. III, we describe the new quantum algorithm to solve the master equation. In Sec. IV, we estimate the quantum resources required for our new algorithm. We focus on the logical T-count and the number of logical qubits, and analyze how they scale with the problem size (e.g., the number of mass bins and time steps). In Sec. V and VI, we discuss implications of our quantum algorithm for the cloud microphysics and conclude the study.

II. FORMULATION

Cloud droplets span a wide range of sizes, from micrometers to millimeters in radius. Their size distribution evolves through the collision-coalescence [29], in which droplets stochastically collide and merge to form larger droplets. Several formulations are used to describe the collision-coalescence, including the stochastic collection equation (SCE), the particle-based methods such as the super-droplet method (SDM), and the master equation [30]. In this study, we adopt the master equation method as a fundamental probabilistic description of the collision-coalescence.

For comparison, we briefly summarize the strengths and limitations of the SCE and the SDM below. The SCE evolves the ensemble-mean droplet size distribution. It is widely used because it provides a computationally efficient description of the collision-coalescence [31]. However, it can predict only the mean behavior and cannot capture realization-to-realization variability due to discrete collisions. In a finite cloud volume, droplet collisions occur as discrete random events, so the size distribution can vary substantially from one realization to another. In particular, rare sequences of collisions can produce unusually large droplets early on and accelerate the growth of the distribution tail [32]. In contrast, the SDM represents collisions stochastically and can capture realization-to-realization variability [19]. However, in SDM, a large droplet population is represented using a finite number of super-droplets with multiplicities, and collisions are realized by stochastic sampling. As a result, statistics of the large-droplet tail are sensitive to the number of super-droplets, because sampling noise decreases only as the particle number increases [32]. As such, both the deterministic mean-field approach (SCE) and the sampling-based particle approach (SDM) cannot directly evolve the full probability distribution of droplet populations.

In contrast, the master equation directly evolves the full probability distribution over droplet populations. Solution of the master equation is computationally challenging for large systems, but it provides an explicit reference of the evolution of probabilities to systematically assess the validity of approximations inherent in the SCE and the SDM [22, 32]. This study tackles this computational challenge by accelerating the solution of the master equation using quantum computing. The remainder

of this section summarizes the formulation of the master equation, following previous studies [21, 22].

We describe the mass distribution of cloud droplets in a discrete and physically intuitive way. We assume that each droplet mass is an integer multiple of the fundamental unit mass, x_1 , which is a physically meaningful minimal mass scale for discretization. With x_1 , the mass of the i -th bin is given by $x_i = ix_1$ ($i = 1, 2, \dots, N$), where N is the total number of bins. The number of droplets in the i -th bin is denoted by n_i . The state of the system we are considering is therefore fully described by the vector $\bar{n} = (n_1, n_2, \dots, n_N)$. In this study, we assume that the total droplet mass x_{total} is conserved throughout the entire time evolution. This assumption allows us to focus on the collision-coalescence process in its simplest form by neglecting sources and sinks of mass due to condensation and evaporation. For simplicity, we also neglect breakups of droplets, so that the evolution is governed solely by coalescence. Here we choose N to satisfy $x_{\text{total}} \leq x_N$. With this choice, droplets with masses larger than x_N can be safely neglected, i.e., $n_j = 0$ ($j > N$).

We denote the probability of a given state as $P(\bar{n})$. Then the master equation governing the time evolution of the state is given by [33]:

$$\begin{aligned} & \frac{\partial P(\bar{n}; t)}{\partial t} \\ &= \sum_{i=1}^N \sum_{j=i+1}^N K(i, j)(n_i + 1)(n_j + 1) \\ & \quad P(\dots, n_i + 1, \dots, n_j + 1, \dots, n_{i+j} - 1, \dots; t) \\ & + \sum_{i=1}^N \frac{1}{2} K(i, i)(n_i + 2)(n_i + 1) \\ & \quad P(\dots, n_i + 2, \dots, n_{2i} - 1, \dots; t) \\ & - \sum_{i=1}^N \sum_{j=i+1}^N K(i, j)n_i n_j P(\bar{n}; t) \\ & - \sum_{i=1}^N \frac{1}{2} K(i, i)n_i(n_i - 1)P(\bar{n}; t). \end{aligned} \quad (1)$$

This equation describes how the rate of change in the probability of a state is determined by the probabilities of the associated states. The first term on the right-hand-side represents the probability gain due to the collision between the i -th and j -th droplets, which results in an increase in the $(i+j)$ -th droplet by one. The second term accounts for the probability gain caused by the collision of two droplets in the i -th bin. The last two terms represent the probability losses from the target state $P(\bar{n})$ due to droplet collisions.

The coefficients in the form of $K(i, j)n_i n_j$ in each term represent transition probabilities. $K(i, j)$ is the collection kernel that represents the probability of collisions between the two droplets of masses x_i and x_j . These coefficients can be separated into two components: the droplet-number-dependent part, $n_i n_j$, and the droplet-

number-independent part, $K(i, j)$. This separation is essentially important for our quantum algorithm and its details will be described later.

The calculation of Eq. (1) is performed for all possible realizations of \bar{n} , and this is computationally challenging. The number of possible states, $R(N)$, grows rapidly with N as is given by the following relation [34]:

$$R(N) \sim \frac{1}{4N\sqrt{3}} \exp\left(\pi\left(\frac{2N}{3}\right)^{1/2}\right). \quad (2)$$

Although classical computers have not allowed performing this calculation for $N > 40$ due to the exponential growth in $R(N)$ [35], quantum computers might have a potential for making it feasible.

In our calculation, the time derivative in Eq. (1) is discretized using a first-order finite difference scheme, following the approach outlined in [22]. A discrete form of the master equation is given by

$$\begin{aligned} & P(\bar{n}; t_0 + \Delta t) \\ &= P(\bar{n}; t_0) \\ & + \Delta t \sum_{i=1}^N \sum_{j=i+1}^N K(i, j)(n_i + 1)(n_j + 1) \\ & \quad P(\dots, n_i + 1, \dots, n_j + 1, \dots, n_{i+j} - 1, \dots; t_0) \\ & + \Delta t \sum_{i=1}^N \frac{1}{2} K(i, i)(n_i + 2)(n_i + 1) \\ & \quad P(\dots, n_i + 2, \dots, n_{2i} - 1, \dots; t_0) \\ & - \Delta t \sum_{i=1}^N \sum_{j=i+1}^N K(i, j)n_i n_j P(\bar{n}; t_0) \\ & - \Delta t \sum_{i=1}^N \frac{1}{2} K(i, i)n_i(n_i - 1)P(\bar{n}; t_0). \end{aligned} \quad (3)$$

The time evolution is calculated step by step using Eq. (3). A sequence of this process allows for the time evolution of the probabilities of all possible states up to the final time T .

Usually, quantities of our interest are not the probabilities themselves, but rather characteristic values derived from the probabilities. For example, the probability of obtaining $n_i = n$ is expressed as

$$P(n_i = n; t) = \sum_{\{n_j\}_{j \neq i}} P(n_1, \dots, n_{i-1}, n_i = n, n_{i+1}, \dots, n_N; t), \quad (4)$$

where the summation is taken n_j for all $j \in \{1, \dots, N\} \setminus \{i\}$. Similarly, the expected number of droplets in the i -th bin can be calculated as

$$\langle n_i \rangle = \sum_n n P(n_i = n; t). \quad (5)$$

A key advantage of our quantum algorithm explained below is that it can compute these characteristic values efficiently.

III. QUANTUM ALGORITHM

A. Quantum state representation

In our algorithm, the probability distribution of droplet mass distributions is encoded in the quantum state $|\psi(t)\rangle_{\mathcal{H}\mathcal{N}}$ as

$$|\psi(t)\rangle_{\mathcal{H}\mathcal{N}} = \sum_{\mathbf{h}} \sum_{\bar{\mathbf{n}}} \sqrt{P(\mathbf{h}, \bar{\mathbf{n}}; t)} |\mathbf{h}\rangle_{\mathcal{H}} |\bar{\mathbf{n}}\rangle_{\mathcal{N}}, \quad (6)$$

where the vector $|\mathbf{h}\rangle_{\mathcal{H}}$ represents the transition history and the vector $|\bar{\mathbf{n}}\rangle_{\mathcal{N}}$ is the mass distribution. The subscripts \mathcal{H} and \mathcal{N} indicate the quantum registers storing these components. The transition history $|\mathbf{h}\rangle_{\mathcal{H}}$ contains details of the sequence of transitions and is expressed as

$$|\mathbf{h}\rangle_{\mathcal{H}} = |h_1, h_2, \dots, h_M\rangle_{\mathcal{H}} = |h_1\rangle_{\mathcal{H}_1} |h_2\rangle_{\mathcal{H}_2} \dots |h_M\rangle_{\mathcal{H}_M}, \quad (7)$$

where M is the total number of time steps, h_m is a transition label at the m -th time step that uniquely specifies the pair of bins involved in the droplet collisions, and the subscript m is an integer index satisfying $1 \leq m \leq M$. The qubits \mathcal{H}_m constitute a quantum register to store the m -th transition history. Generally, \mathcal{H}_m does not consist of a single qubit, but the number of qubits used for \mathcal{H}_m is approximately equal to the logarithm of the total number of transition labels. The detail of this count will be described in Sec. IV. Similarly, the mass distribution $|\bar{\mathbf{n}}\rangle_{\mathcal{N}}$ is given by

$$|\bar{\mathbf{n}}\rangle_{\mathcal{N}} = |n_1, n_2, \dots, n_N\rangle_{\mathcal{N}} = |n_1\rangle_{\mathcal{N}_1} |n_2\rangle_{\mathcal{N}_2} \dots |n_N\rangle_{\mathcal{N}_N}. \quad (8)$$

Let $P(\mathbf{h}, \bar{\mathbf{n}}; t)$ indicate the probability for the system to be in a combined state denoted by \mathbf{h} and $\bar{\mathbf{n}}$ at time t . Taking the sum of $P(\mathbf{h}, \bar{\mathbf{n}}; t)$ with respect to h , we obtain the following relation:

$$P(\bar{\mathbf{n}}; t) = \sum_{\mathbf{h}} P(\mathbf{h}, \bar{\mathbf{n}}; t). \quad (9)$$

For simplicity, we consider a closed system in which the total mass $x_{\text{total}} = x_N$ is conserved, and we assume an initial condition where all droplets reside in the first bin. Thus, $n_1 = x_{\text{total}}/x_1 = N$, and the probability of the initial state is $P(n_1 = N, n_2 = 0, \dots, n_N = 0; t = 0) = 1$. The corresponding quantum state is given by

$$|\psi(0)\rangle_{\mathcal{H}\mathcal{N}} = |\mathbf{0}\rangle_{\mathcal{H}} |N\rangle_{\mathcal{N}_1} |0\rangle_{\mathcal{N}_2} \dots |0\rangle_{\mathcal{N}_N}, \quad (10)$$

where $|\mathbf{0}\rangle_{\mathcal{H}} = |0\rangle_{\mathcal{H}_1} |0\rangle_{\mathcal{H}_2} \dots |0\rangle_{\mathcal{H}_M}$ represents the initial transition history with no transitions.

B. Probability division

The time evolution of the probability distribution of cloud droplet masses can be obtained by tracking the

time evolution of the probability amplitudes of the quantum state. The calculation progresses by redistributing the probabilities according to the transition labels at each time step. This redistribution process for all possible states is referred to as the *probability division* in this study. For example, at one time step Δt after the initial state, the quantum state Eq. (10) becomes

$$\begin{aligned} & |\psi(\Delta t)\rangle_{\mathcal{H}\mathcal{N}} \\ &= \sqrt{1 - \frac{1}{2}K(1, 1)N(N-1)\Delta t} \\ & \quad |0\rangle_{\mathcal{H}_1} |0\rangle_{\mathcal{H}_2} \dots |0\rangle_{\mathcal{H}_M} |N\rangle_{\mathcal{N}_1} |0\rangle_{\mathcal{N}_2} \dots |0\rangle_{\mathcal{N}_N} \\ & \quad + \sqrt{\frac{1}{2}K(1, 1)N(N-1)\Delta t} \\ & \quad |1\rangle_{\mathcal{H}_1} |0\rangle_{\mathcal{H}_2} \dots |0\rangle_{\mathcal{H}_M} |N-2\rangle_{\mathcal{N}_1} |1\rangle_{\mathcal{N}_2} \dots |0\rangle_{\mathcal{N}_N}. \end{aligned} \quad (11)$$

In this first step, we can limit the probability division to the collision of two droplets in the first bin. We label this transition as 1. We reserve the label 0 for the no-transition case. The numbering rule of the transition labels will be explained later.

Figure 1 schematically shows the sequence of the probability divisions for multiple steps starting from the initial state. This includes both the collision transitions (with labels $h \geq 1$) and the non-collision holding events ($h = 0$).

A quantum advantage is expected from this probability division. In the classical algorithm, the probability division must be performed for all possible states sequentially. This results in exponential growth of computational costs as the number of possible states increases as Eq. (2). In contrast, the quantum computing can process these state transitions simultaneously. Leveraging the quantum superposition, a single probability division applies to all possible states at once, and thus, the repeated application of the probability division can be eliminated. This is one of the key advantages of our quantum algorithm in this problem. Handling all states in parallel can significantly reduce computational costs. In the following paragraphs, we will explain how a single time step is implemented in the probability division.

To go one step forward, the probability division is performed for all possible states for all possible transitions.

For example, the probability flow from the state $(n_1 = N-2, n_2 = 1, n_3 = 0, \dots)$ to $(n_1 = N-3, n_2 = 0, n_3 = 1, \dots)$ and from the state $(n_1 = N-4, n_2 = 2, n_3 = 0, \dots)$ to $(n_1 = N-5, n_2 = 1, n_3 = 1, \dots)$ are conducted simultaneously because both are associated with collisions between droplets in the first and the second bins to create droplets in the third bin. By doing this, the probability division can be calculated simultaneously for all possible states for the same transition label.

The probability division is conducted sequentially for all possible pair of bins (Fig. 2). Each transition is labeled by h , and the corresponding transition probability from the state $\bar{\mathbf{n}}$ is written as $r_h(\bar{\mathbf{n}})$. The label h ranges from 0 to H , where H is the total number of possible bin

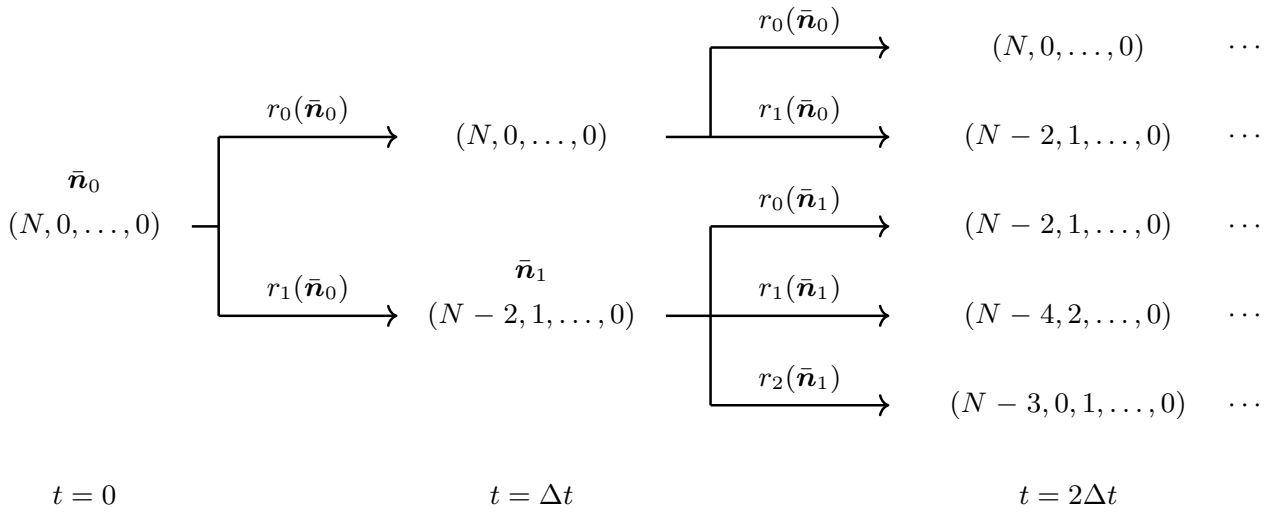


FIG. 1. The schematic diagram of the probability division process over multiple steps. The numbers in parentheses represent the mass distribution $\bar{\mathbf{n}}$. For convenience, the states $(N, 0, \dots, 0)$ are denoted as $\bar{\mathbf{n}}_0$, and $(N - 2, 1, \dots, 0)$ as $\bar{\mathbf{n}}_1$. The arrows indicate the probability flow. The transition probability from the state $\bar{\mathbf{n}}_i$ by the transition labeled h is denoted as $r_h(\bar{\mathbf{n}}_i)$ above the arrows. The probability of no transition is represented by r_0 . The transition probabilities associated with the transitions with labels 1 and 2 are denoted as r_1 and r_2 , respectively.

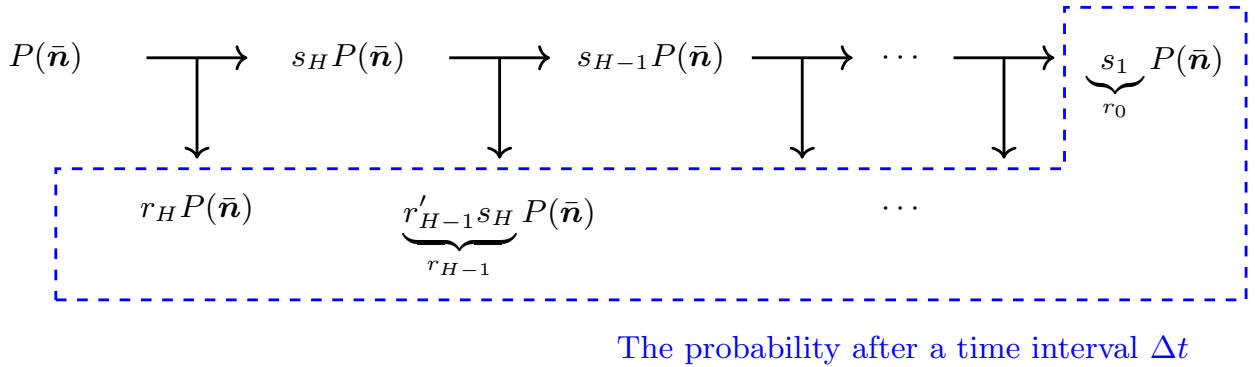


FIG. 2. The schematic diagram of the probability division process for a single time step. The probability $P(\bar{\mathbf{n}})$ is first divided into $s_H P(\bar{\mathbf{n}})$ and $r_H P(\bar{\mathbf{n}})$, where r_H is the transition probability associated with the transition H , and s_H is the remaining part of this probability division ($s_H = 1 - r_H$). Similarly, the probability division following the transition $(H - 1)$ is conducted, and $s_H P(\bar{\mathbf{n}})$ is divided into $s_{H-1} P(\bar{\mathbf{n}})$ and $r'_{H-1} P(\bar{\mathbf{n}})$. After performing the probability division for every possible pair of bins, the probabilities at the next time level are obtained (indicated by the blue dots).

pairs. The correspondence between each bin pair and its transition label h can be arbitrary, as long as it is uniquely defined. The case with no collisions, in which the state remains unchanged, is treated separately. This no-transition case is computed as the complement of all other transition probabilities, and is assigned the label 0. In addition to the transition probability $r_h(\bar{\mathbf{n}})$, we introduce another quantity $s_h(\bar{\mathbf{n}})$ to describe the intermediate state of the system during the sequential execution of probability divisions. It represents the fraction of the probability retained in the state $\bar{\mathbf{n}}$ after the probability division corresponding to a transition labeled h , and

satisfies the relationship

$$s_h(\bar{\mathbf{n}}) = 1 - \sum_{k=h}^H r_k(\bar{\mathbf{n}}), \quad (12)$$

where the index k runs from h to H because the probability division is executed in descending order, starting from the transition labeled H . We introduce the modified transition probability $r'_h(\bar{\mathbf{n}})$ to calculate the transition probability $r_h(\bar{\mathbf{n}})$ from the remaining probability $s_{h+1}(\bar{\mathbf{n}})$. This modified transition probability is defined as

$$r'_h(\bar{\mathbf{n}}) = \frac{r_h(\bar{\mathbf{n}})}{s_{h+1}(\bar{\mathbf{n}})}. \quad (13)$$

By using these notations, as summarized in Fig. 2, the sequence of the probability division for one time step can be described as

$$\begin{aligned}
P(\bar{n}) &\rightarrow r_H P(\bar{n}) + s_H P(\bar{n}) \\
&\rightarrow r_H P(\bar{n}) + r'_{H-1} s_H P(\bar{n}) + (1 - r'_{H-1}) s_H P(\bar{n}) \\
&= r_H P(\bar{n}) + r_{H-1} P(\bar{n}) + s_{H-1} P(\bar{n}) \\
&\rightarrow \dots \\
&\rightarrow r_H P(\bar{n}) + r_{H-1} P(\bar{n}) + \dots + s_1 P(\bar{n}) \\
&= \sum_{k=0}^H r_k P(\bar{n}) \quad (\because s_1 = r_0),
\end{aligned} \tag{14}$$

where each arrow stands for a probability division associated with a transition label.

C. Quantum circuits

In our quantum algorithm, one time step is constructed by a sequential application of the quantum operations that perform the probability division for each bin pair. These quantum operations consist of four main components. The first is the calculation of the quantities r'_h and s_h using fixed-point quantum arithmetic. Its details are provided in Appendix A. This component is realized by the quantum gate $U_P(h)$. The second is the application of the calculated transition probability r'_h to change the quantum phase through controlled phase gates. This component is realized by the quantum gate U_{\sin} . The third is the uncomputation of the auxiliary qubits, which is realized by $U_Q(h)$. Here, “uncomputation” means reversing previously performed computations to restore qubits to their original states. This process is required to reuse qubits for repeated calculations because qubits cannot be directly reset unlike in classical computing. The last component is a controlled adder gate U_{add} , which updates the history register to keep track of the application order of probability divisions. In the following paragraphs, we will explain the brief overview of each component. Refer to Appendix B for detailed explanations of the U_P , U_{\sin} , U_Q , and U_{add} gates.

The $U_P(h)$ gate calculates the pieewise arcsine of the square root of a modified transition probability r'_h , i.e., $\arcsin \sqrt{r'_h}$. This value is computed because the quantum phase gate $R_y(\theta)$, which is applied inside the U_{\sin} gate, is expressed as

$$R_y(\theta) = \begin{pmatrix} \cos \frac{\theta}{2} & -\sin \frac{\theta}{2} \\ \sin \frac{\theta}{2} & \cos \frac{\theta}{2} \end{pmatrix}, \tag{15}$$

and operates like $R_y(2 \arcsin \sqrt{r'_h}) |0\rangle = \sqrt{1 - r'_h} |0\rangle + \sqrt{r'_h} |1\rangle$. The value r'_h can be computed as long as $i(h), j(h), n_{i(h)}, n_{j(h)}$ and s_{h+1} are given. Here $i(h)$ and $j(h)$ are the indices of the bins that are collided in the

transition labeled h . Therefore, the $U_P(h)$ gate acts as

$$\begin{aligned}
U_P(h) &: |n_{i(h)}\rangle_{\mathcal{N}_{i(h)}} |n_{j(h)}\rangle_{\mathcal{N}_{j(h)}} |s_{h+1}\rangle_{\mathcal{A}} |0\rangle_{\mathcal{B}} |0\rangle_{\mathcal{C}} \\
&\mapsto |n_{i(h)}\rangle_{\mathcal{N}_{i(h)}} |n_{j(h)}\rangle_{\mathcal{N}_{j(h)}} |s_{h+1}\rangle_{\mathcal{A}} |\text{pp}_{\arcsin} \sqrt{r'_h}\rangle_{\mathcal{B}} |\lambda\rangle_{\mathcal{C}},
\end{aligned} \tag{16}$$

where $|\lambda\rangle$ is an auxiliary state used during the computation of $\text{pp}_{\arcsin} \sqrt{r'_h}$ and is a composite state comprising both integer and real numbers. The symbol pp_{\arcsin} means the piecewise polynomial to calculate arcsine [36]. \mathcal{A} , \mathcal{B} , and \mathcal{C} are the quantum registers: \mathcal{A} is used to store s_{h+1} , \mathcal{B} is used to store the calculated result of $\text{pp}_{\arcsin} \sqrt{r'_h}$, and \mathcal{C} is used to store the auxiliary states. While the number of droplets in the i -th bin, n_i , is an integer stored in binary form in the qubit \mathcal{N}_i , the values of s_{h+1} and $\text{pp}_{\arcsin} \sqrt{r'_h}$ are real numbers represented in the fixed-point form in the qubits \mathcal{A} and \mathcal{B} , respectively. These real numbers lie within the ranges $[0, 1]$ and $[0, \pi/2]$, respectively, and can be expressed with a precision of n bits as

$$\alpha = \alpha_{n-1} 2^0 + \alpha_{n-2} 2^{-1} + \dots + \alpha_0 2^{-n+1}, \tag{17}$$

where α represents either s_{h+1} or $\text{pp}_{\arcsin} \sqrt{r'_h}$, and $\alpha_i \in \{0, 1\} (i = 0, 1, \dots, n-1)$. This value is encoded in the quantum register as

$$|\alpha\rangle = |\alpha_{n-1}\rangle |\alpha_{n-2}\rangle \dots |\alpha_0\rangle. \tag{18}$$

Here, $|1.0\rangle$ is defined to represent $|1\rangle |0\rangle \dots |0\rangle$ for convenience.

Further details of this representation and its implementation are provided in Appendix B.

The U_{\sin} gate applies the probability division to the quantum phase, using the result of the first component. The controlled phase gates enable this operation. The U_{\sin} gate acts as

$$\begin{aligned}
U_{\sin} &: |0\rangle_{\mathcal{H}_m} |\text{pp}_{\arcsin} \sqrt{r'_h}\rangle_{\mathcal{B}} \\
&\mapsto \left[\sqrt{1 - r'_h} |0\rangle_{\mathcal{H}_m} + \sqrt{r'_h} |1\rangle_{\mathcal{H}_m} \right] |\text{pp}_{\arcsin} \sqrt{r'_h}\rangle_{\mathcal{B}},
\end{aligned} \tag{19}$$

where \mathcal{H}_m is the quantum register storing the transition label at the m -th time step. Notably, the U_{\sin} gate is applied only when the quantum register \mathcal{H}_m is in the $|0\rangle_{\mathcal{H}_m}$ state. That is, the probability division is applied only to a fraction of the probability that has not yet been affected by any previous transition rules in the m -th time step.

After completing the probability division for the transition label h , the auxiliary states stored in the qubits \mathcal{B} and \mathcal{C} are uncomputed, and the value of s_{h+1} is updated to s_h , which is used in the probability division in the next transition ($h-1$). This is achieved by applying the

$U_Q(h)$ gate as

$$U_Q(h) : |n_{i(h)}\rangle_{\mathcal{N}_{i(h)}} |n_{j(h)}\rangle_{\mathcal{N}_{j(h)}} |s_{h+1}\rangle_{\mathcal{A}} |\text{PParcsin}\sqrt{r'_h}\rangle_{\mathcal{B}} |\lambda\rangle_{\mathcal{C}} \\ \mapsto |n_{i(h)}\rangle_{\mathcal{N}_{i(h)}} |n_{j(h)}\rangle_{\mathcal{N}_{j(h)}} |s_h\rangle_{\mathcal{A}} |0\rangle_{\mathcal{B}} |0\rangle_{\mathcal{C}}. \quad (20)$$

In addition to the uncomputation, controlled addition is applied on the quantum register \mathcal{H}_m . Specifically, this operation maps $|h\rangle_{\mathcal{H}_m}$ to $|h+1\rangle_{\mathcal{H}_m}$ only when $h \geq 1$, while $|0\rangle_{\mathcal{H}_m}$ remains unchanged. This step is used to keep track of whether the probability division has already been applied to a given state, and to record the transition label used to update the state.

As noted earlier, the probability divisions are applied in descending order from $h = H$ down to $h = 1$. When a state is first updated at index h , its history register is set to 1. In each subsequent step, the register is incremented by 1. Therefore, once all divisions have been completed, the final value of the history register becomes equal to the transition label at which the state was updated. This operation is implemented using the U_{add} gate.

D. Quantum circuit for one time step

The the quantum circuit to perform a probability division for one time step is explained. This is the case of applying the transition labeled h at the m -th time step. Just before this probability division, the quantum state is

$$\sum_{h_1, \dots, h_{m-1}} \sum_{\bar{\mathbf{n}}} |h_1\rangle_{\mathcal{H}_1} \dots |h_{m-1}\rangle_{\mathcal{H}_{m-1}} \\ \left[\sum_{k=h+1}^H \sqrt{r_k P(\mathbf{h}, \bar{\mathbf{n}}; (m-1)\Delta t)} |k-h+1\rangle_{\mathcal{H}_m} \right. \\ \left. + \sqrt{s_{h+1} P(\mathbf{h}, \bar{\mathbf{n}}; (m-1)\Delta t)} |0\rangle_{\mathcal{H}_m} \right] \\ |0\rangle_{\mathcal{H}_{m+1}} \dots |0\rangle_{\mathcal{H}_M} |\bar{\mathbf{n}}\rangle_{\mathcal{N}} |s_{h+1}\rangle_{\mathcal{A}}. \quad (21)$$

By sequentially applying the $U_P(h)$, U_{sin} , and $U_Q(h)$ gates defined by Eqs. (16), (19), and (20), respectively, the probability division for the transition labeled h trans-

forms the quantum state Eq. (21) into the following:

$$\sum_{h_1, \dots, h_{m-1}} \sum_{\bar{\mathbf{n}}} |h_1\rangle_{\mathcal{H}_1} \dots |h_{m-1}\rangle_{\mathcal{H}_{m-1}} \\ \left[\sum_{k=h+1}^H \sqrt{r_k P(\mathbf{h}, \bar{\mathbf{n}}; (m-1)\Delta t)} |k-h+1\rangle_{\mathcal{H}_m} \right. \\ \left. + \sqrt{r'_h s_{h+1} P(\mathbf{h}, \bar{\mathbf{n}}; (m-1)\Delta t)} |1\rangle_{\mathcal{H}_m} \right. \\ \left. + \sqrt{(1-r'_h) s_{h+1} P(\mathbf{h}, \bar{\mathbf{n}}; (m-1)\Delta t)} |0\rangle_{\mathcal{H}_m} \right] \\ |0\rangle_{\mathcal{H}_{m+1}} \dots |0\rangle_{\mathcal{H}_M} |\bar{\mathbf{n}}\rangle_{\mathcal{N}} |s_h\rangle_{\mathcal{A}} \\ = \sum_{h_1, \dots, h_{m-1}} \sum_{\bar{\mathbf{n}}} |h_1\rangle_{\mathcal{H}_1} \dots |h_{m-1}\rangle_{\mathcal{H}_{m-1}} \\ \left[\sum_{k=h}^H \sqrt{r_k P(\mathbf{h}, \bar{\mathbf{n}}; (m-1)\Delta t)} |k-h+1\rangle_{\mathcal{H}_m} \right. \\ \left. + \sqrt{s_h P(\mathbf{h}, \bar{\mathbf{n}}; (m-1)\Delta t)} |0\rangle_{\mathcal{H}_m} \right] \\ |0\rangle_{\mathcal{H}_{m+1}} \dots |0\rangle_{\mathcal{H}_M} |\bar{\mathbf{n}}\rangle_{\mathcal{N}} |s_h\rangle_{\mathcal{A}}. \quad (22)$$

Subsequently, the U_{add} gate is applied to increment the transition history qubits by one. As a result, the resulting quantum state becomes

$$\sum_{h_1, \dots, h_{m-1}} \sum_{\bar{\mathbf{n}}} |h_1\rangle_{\mathcal{H}_1} \dots |h_{m-1}\rangle_{\mathcal{H}_{m-1}} \\ \left[\sum_{k=h}^H \sqrt{r_k P(\mathbf{h}, \bar{\mathbf{n}}; (m-1)\Delta t)} |k-h+2\rangle_{\mathcal{H}_m} \right. \\ \left. + \sqrt{s_h P(\mathbf{h}, \bar{\mathbf{n}}; (m-1)\Delta t)} |0\rangle_{\mathcal{H}_m} \right] \\ |0\rangle_{\mathcal{H}_{m+1}} \dots |0\rangle_{\mathcal{H}_M} |\bar{\mathbf{n}}\rangle_{\mathcal{N}} |s_h\rangle_{\mathcal{A}}. \quad (23)$$

Series of these four components are sequentially applied for all of the possible bin pairs. After completing all probability divisions in the m -th time step, the quantum register \mathcal{A} holds the value $|s_1\rangle_{\mathcal{A}}$. To reuse \mathcal{A} in the next time step, this state $|s_1\rangle_{\mathcal{A}}$ must be uncomputed back to the initial state $|1.0\rangle_{\mathcal{A}}$. This is achieved by iteratively applying the $U_R(h)$ gate, which acts as the inverse of the combined operations of $U_Q(h)$ and $U_P(h)$. Additionally, the states that have non-zero transition labels require an update of the mass distribution to the post-collision state. For example, if the transition label corresponds to a collision between droplets in the first bin, and the current state is $|N\rangle_{\mathcal{N}_1} |0\rangle_{\mathcal{N}_2} \dots |0\rangle_{\mathcal{N}_N}$, it must be updated to $|N-2\rangle_{\mathcal{N}_1} |1\rangle_{\mathcal{N}_2} \dots |0\rangle_{\mathcal{N}_N}$. This update is performed using the U_{shift} gate, which consists of constant additions and subtractions. Details of $U_R(h)$ and U_{shift} gates are explained in Appendix B.

The complete set of operations for a single time step is summarized in the quantum circuit in Fig. 3. The operator for calculating a single time step is denoted as $U_{\Delta t}$ on the left-hand-side. This operator such that $U_{\Delta t} |\psi((m-1)\Delta t)\rangle_{\mathcal{H}_N} |1.0\rangle_{\mathcal{A}} |0\rangle_{\mathcal{B}} |0\rangle_{\mathcal{C}} = |\psi(m\Delta t)\rangle_{\mathcal{H}_N} |1.0\rangle_{\mathcal{A}} |0\rangle_{\mathcal{B}} |0\rangle_{\mathcal{C}}$.

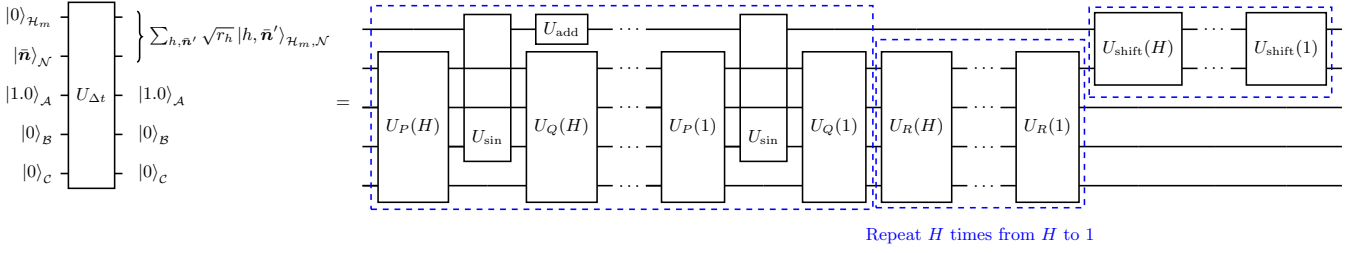


FIG. 3. The quantum circuit for a single time step. The left-hand-side of the equation is the input and output states of the time step, while the right-hand-side illustrates the detailed operations within the time step. These segments enclosed by blue dashed lines on the right-hand-side include sequential applications of probability division for all possible bin pairs (omitted for simplicity, represented by dots in the figure). The left one calculates the modified transition probability and applies the probability division to the quantum phase. The central one uncomputes the auxiliary qubits \mathcal{A} to $|1.0\rangle_{\mathcal{A}}$. The right one updates the mass distribution $|\bar{n}\rangle_{\mathcal{N}}$ to the next time step based on the transition label $|h\rangle_{\mathcal{H}_m}$.

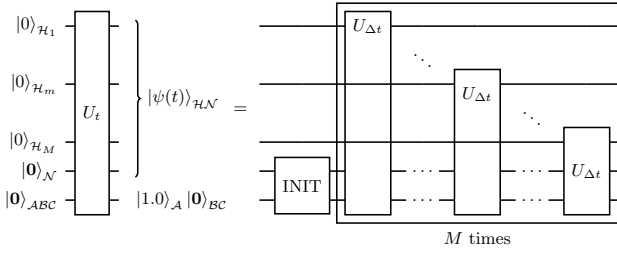


FIG. 4. The quantum circuit for calculating the time evolution of the probability distribution over all time steps. The circuit begins with the initialization of the droplet mass distribution and the auxiliary qubits \mathcal{A} in the state $|1.0\rangle_{\mathcal{A}}$. Subsequently, the quantum gates $U_{\Delta t}$ are sequentially applied M times. The transition history qubits \mathcal{H}_m is used for the m -th time step.

E. Quantum circuit for full time steps

The quantum circuit for the computation of the entire time evolution is shown in Fig. 4. The process begins by initializing the quantum registers to the states of the initial conditions. This initialization is performed by simply applying the NOT gates. After the initialization, the probability division for each time step is carried out sequentially. As the time proceeds, the target qubits of the controlled phase gate change from \mathcal{H}_1 to \mathcal{H}_M . The operator for calculating the final state is denoted as U_t on the left-hand-side. This operates such that $U_t |0\rangle_{\mathcal{H}\mathcal{N}} |0\rangle_{\mathcal{A}} |0\rangle_{\mathcal{B}} |0\rangle_{\mathcal{C}} = |\psi(t)\rangle_{\mathcal{H}\mathcal{N}} |1.0\rangle_{\mathcal{A}} |0\rangle_{\mathcal{B}} |0\rangle_{\mathcal{C}}$.

F. Quantum circuit for postprocessing

After the time evolution is finished, we derive characteristic values from the quantum state $|\psi(t)\rangle_{\mathcal{H}\mathcal{N}}$ at the final step. Since the quantum state is expressed as in Eqs. (6), (7), and (8), the characteristic values can be obtained efficiently. For example, the probability of observing $n_i = n$ in Eq. (4) is encoded directly in the quan-

tum amplitude of $|n\rangle_{\mathcal{N}_i}$. This can be verified as

$$\begin{aligned}
 P(n_i = n; t) &= \sum_{\mathbf{h}} \sum_{\text{Except } n_i} P(\mathbf{h}, n_1, \dots, n_i = n, \dots, n_N; t) \\
 &= \left\| \sum_{\mathbf{h}} \sum_{\text{Except } n_i} \sqrt{P(\mathbf{h}, n_1, \dots, n_i = n, \dots, n_N; t)} \right. \\
 &\quad \left. |\mathbf{h}\rangle_{\mathcal{H}} |n_1\rangle_{\mathcal{N}_1} \dots |n_i\rangle_{\mathcal{N}_i} \dots |n_N\rangle_{\mathcal{N}_N} \right\|^2 \\
 &= \|I_{\text{Except } \mathcal{N}_i} \otimes \langle n |_{\mathcal{N}_i} |\psi(t)\rangle_{\mathcal{H}\mathcal{N}} \|^2, \tag{24}
 \end{aligned}$$

where $I_{\text{Except } \mathcal{N}_i}$ is the identity operator acting on all qubits except \mathcal{N}_i . We can use the quantum amplitude estimation [26, 27] for an efficient estimation of $P(n_i = n; t)$.

The expected values of the number of droplets in the i -th bin defined in Eq. (5) can also be estimated by the quantum amplitude estimation. The expected values can be calculated by applying controlled phase gates $U_c(i)$ sequentially. The $U_c(i)$ is defined to encode the number of droplets in the i -th bin into the quantum amplitude as follows:

$$U_c(i) : |0\rangle_{\mathcal{D}} |n_i\rangle_{\mathcal{N}_i} \mapsto \left[\sqrt{\frac{n_i}{d}} |0\rangle_{\mathcal{D}} + \sqrt{1 - \frac{n_i}{d}} |1\rangle_{\mathcal{D}} \right] |n_i\rangle_{\mathcal{N}_i}, \tag{25}$$

where d is a value larger than the maximum number of droplets in the i -th bin, and \mathcal{D} is an auxiliary qubit. In this work, we use $d = 2^{q_i}$, where q_i denotes the number of qubits required to store the quantum state $|n_i\rangle_{\mathcal{N}_i}$. The detailed algorithm for the construction of U_c is explained in Appendix B. Figure 5 is a quantum circuit to obtain the final state expressed as

$$|\psi_{\text{final}}\rangle_{\mathcal{D}\mathcal{H}\mathcal{N}} = \sum_{\mathbf{h}} \sum_{\bar{n}} \left[\sqrt{\frac{n_i}{d}} |0\rangle_{\mathcal{D}} + \sqrt{1 - \frac{n_i}{d}} |1\rangle_{\mathcal{D}} \right] \sqrt{P(\mathbf{h}, \bar{n}; t)} |\mathbf{h}\rangle_{\mathcal{H}} |\bar{n}\rangle_{\mathcal{N}}. \tag{26}$$

Therefore, the expected value of the number of droplets in the i -th bin can be obtained by measuring the proba-

bility of obtaining the quantum state $|0\rangle_{\mathcal{D}}$ as

$$\begin{aligned} \langle n_i \rangle &= d \sum_{n_i} \frac{n_i}{d} P(n_i = n; t) \\ &= d \left\| \sum_{n_i} \sqrt{\frac{n_i}{d}} \sum_{\mathbf{h}} \sum_{\text{Except } n_i} \sqrt{P(\mathbf{h}, \bar{\mathbf{n}}; t)} |\mathbf{h}\rangle_{\mathcal{H}} |\bar{\mathbf{n}}\rangle_{\mathcal{N}} \right\|^2 \\ &= d \| I_{\mathcal{HN}} \otimes \langle 0 |_{\mathcal{D}} |\psi_{\text{final}}\rangle_{\mathcal{DHN}} \|^2, \end{aligned} \quad (27)$$

and the quantum amplitude estimation allows an efficient estimation of this value.

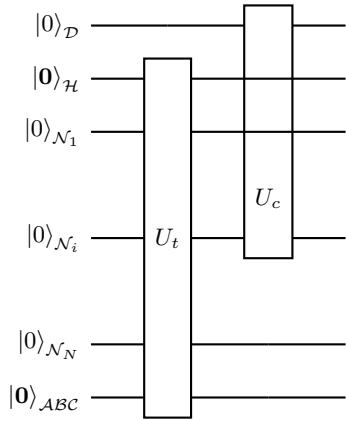


FIG. 5. The quantum circuit for calculating the expected value of the number of droplets in the i -th bin. The expected value is encoded into the quantum amplitude of the auxiliary qubit \mathcal{D} .

IV. QUANTUM RESOURCE ESTIMATES

The quantum resources required for our algorithm are estimated to assess its feasibility on fault-tolerant quantum computers and to identify the dominant cost drivers. In general, we can assume that the resources are primarily dependent on the number of logical qubits and the number of quantum gates. In this study, we count the number of logical qubits for representing the quantum state $|\psi(t)\rangle$ and the number of auxiliary qubits for each operation. As for the quantum gates, we focus on counting the number of T gates, as the T gate requires significantly more time than Clifford gates [37].

We count the number of gates for a single operation of $U_P, U_{\sin}, U_Q, U_{\text{add}}, U_R$, and U_{shift} , respectively, and multiply them by the number of times each operation is called.

First, we count the number of logical qubits for the quantum state $|\psi(t)\rangle$. The quantum state $|\psi(t)\rangle$ is given by Eqs. (6), (7), and (8). In the current setup, the total mass is equivalent to the mass of the largest droplets x_N . Thus, the maximum number of droplets in the i -th bin is given by $I = \lfloor N/i \rfloor$, where $\lfloor * \rfloor$ is the greatest integer less than or equal to $*$. The number of logical qubits required

for $|n_i\rangle_{\mathcal{N}_i}$ is calculated as $q_i = \lceil \log_2(\lfloor N/i \rfloor + 1) \rceil$, where $\lceil * \rceil$ is the smallest integer greater than or equal to $*$. Consequently, the total number of logical qubits required for the quantum state $|\bar{\mathbf{n}}\rangle_{\mathcal{N}}$ is given by

$$q_{\text{count}}(\mathcal{N}) = \sum_{i=1}^N \lceil \log_2(\lfloor N/i \rfloor + 1) \rceil, \quad (28)$$

where $q_{\text{count}}(*)$ denotes the number of logical qubits required for the quantum register $*$. The number of logical qubits required for the quantum state $|h_m\rangle_{\mathcal{H}_m}$ can be calculated from the total number of possible bin pairs H . From Eq. (3) and the conservation of total mass,

$$H = \begin{cases} \sum_{i=1}^{N/2-1} \sum_{j=i+1}^{N-i} 1 + \sum_{i=1}^{N/2} 1 = \frac{N^2}{4} & (N : \text{even}), \\ \sum_{i=1}^{(N-1)/2} \sum_{j=i+1}^{N-i} 1 + \sum_{i=1}^{(N-1)/2} 1 = \frac{N^2-1}{4} & (N : \text{odd}). \end{cases} \quad (29)$$

The number of logical qubits required for $|h_m\rangle_{\mathcal{H}_m}$ is $q_h = \lceil \log_2(\lfloor H \rfloor + 1) \rceil$. Note that this number is the same across all time steps. Therefore, the total number of logical qubits required for the quantum state $|\mathbf{h}\rangle_{\mathcal{H}}$ is calculated as

$$q_{\text{count}}(\mathcal{H}) = M \lceil \log_2(\lfloor H \rfloor + 1) \rceil. \quad (30)$$

Next, we consider the number of auxiliary qubits in the quantum circuit. The auxiliary qubits $\mathcal{A}, \mathcal{B}, \mathcal{C}$, and \mathcal{D} , which are used in the computation, play different roles. \mathcal{A} stores the remaining probability s_h , \mathcal{B} stores $\text{pp}_{\arcsin} \sqrt{r'_h}$, \mathcal{C} stores auxiliary states during computation, and \mathcal{D} encodes the phase related to the expected value. The numbers of qubits required for these auxiliary registers are as follows:

$$q_{\text{count}}(\mathcal{A}) = n_\epsilon, \quad (31)$$

$$q_{\text{count}}(\mathcal{B}) = n_\epsilon, \quad (32)$$

$$q_{\text{count}}(\mathcal{C}) = 3q_1 + 5n_\epsilon + 1, \text{ and} \quad (33)$$

$$q_{\text{count}}(\mathcal{D}) = 1, \quad (34)$$

where n_ϵ is the number of qubits for encoding the piecewise arcsine of the square root of the transition probability r'_h , and q_1 is the number of qubits for the first bin. In addition to these, the auxiliary qubits for quantum arithmetic operations must also be taken into account. The details of the qubits count for these auxiliary qubits are explained in Appendix B.

As for the number of T gates, the detailed algorithms and the resources for each operation are provided in Appendix B. In summary, the number of T gates required

for each operation is as follows:

$$\begin{aligned}
T_{\text{count}}(U_P) = & T_{\text{count}}(\text{MUL_INT}_{q_1, q_1}) \\
& + T_{\text{count}}(\text{MUL_CONST_INT_UI}_{2q_1, n_\epsilon}) \\
& + T_{\text{count}}(\text{COMP}_{n_\epsilon}) \\
& + 2T_{\text{count}}(\text{c-SUB}_{n_\epsilon}) \\
& + 2T_{\text{count}}(\text{SQRT}_{n_\epsilon}) + T_{\text{count}}(\text{DIV}_{n_\epsilon}) \\
& + T_{\text{count}}(\text{ARCSIN}_{n_\epsilon, \epsilon_{\text{arcsin}}}), \quad (35)
\end{aligned}$$

$$T_{\text{count}}(U_{\text{sin}}) = 12n_\epsilon + 6.6 \log_2(4/\epsilon_{\text{sin}}) + 8q_h - 16, \quad (36)$$

$$\begin{aligned}
T_{\text{count}}(U_Q) = & T_{\text{count}}(\text{MUL_INT}_{q_1, q_1}) \\
& + T_{\text{count}}(\text{MUL_CONST_INT_UI}_{2q_1, n_\epsilon}) \\
& + T_{\text{count}}(\text{COMP}_{n_\epsilon}) \\
& + 2T_{\text{count}}(\text{c-SUB}_{n_\epsilon}) \\
& + 2T_{\text{count}}(\text{SQRT}_{n_\epsilon}) + T_{\text{count}}(\text{DIV}_{n_\epsilon}) \\
& + T_{\text{count}}(\text{ARCSIN}_{n_\epsilon, \epsilon_{\text{arcsin}}}) \\
& + T_{\text{count}}(\text{SUB}_{n_\epsilon}), \quad (37)
\end{aligned}$$

$$\begin{aligned}
T_{\text{count}}(U_{\text{add}}) = & T_{\text{count}}(\text{ADD_CONST}_{q_h}) \\
& + T_{\text{count}}(\text{Toffoli}_{q_h}), \quad (38)
\end{aligned}$$

$$\begin{aligned}
T_{\text{count}}(U_R) = & 2T_{\text{count}}(\text{MUL_INT}_{q_1, q_1}) \\
& + 2T_{\text{count}}(\text{MUL_CONST_INT_UI}_{2q_1, n_\epsilon}) \\
& + T_{\text{count}}(\text{ADD}_{n_\epsilon}), \quad (39)
\end{aligned}$$

$$T_{\text{count}}(U_{\text{shift}}) = \begin{cases} \begin{aligned} & 2T_{\text{count}}(\text{Toffoli}_{q_h}) + T_{\text{count}}(\text{c-ADD}_{q_i+j}) \\ & + T_{\text{count}}(\text{c-SUB}_{q_i}) + T_{\text{count}}(\text{c-SUB}_{q_j}) \end{aligned} & \text{(case 1),} \\ \begin{aligned} & 2T_{\text{count}}(\text{Toffoli}_{q_h}) + T_{\text{count}}(\text{c-ADD}_{q_{2i}}) \\ & + T_{\text{count}}(\text{c-SUB}_{q_i}) \end{aligned} & \text{(case 2),} \end{cases} \quad (40)$$

where $T_{\text{count}}(*)$ denotes the total number of T gates used in the operation $*$. The number of T gates for U_{shift} depends on the pair of bins in the collision. In case 1 of Eq. (40), the transition is due to a collision between a pair of droplets of different masses, whereas in case 2, it is due to a collision between a pair of droplets of equal mass. In the operation of $U_{\Delta t}$, the number of calls for each component, except for the U_{add} gate, corresponds to the total number of pair of bins H , as illustrated in the quantum circuit in Fig. 3. The U_{add} gate is called $H - 1$ times because there is no need to add the value 1 at the final division. The $U_{\Delta t}$ operation is performed M times inside U_t , as shown in the quantum circuit in Fig. 4. Consequently, the total number of T gates required for U_t is obtained by multiplying the number of T gates required in each operation by the number of times each operation is called.

The cost of implementing U_c is detailed in Appendix B. Specifically, it is given by

$$T_{\text{count}}(U_c) = 1.15I \log_2(I/\epsilon_c), \quad (41)$$

where I is the maximum number of droplets in a bin, and ϵ_c is the precision parameter for the phase gate.

The number of times that U_t and U_c are called depends on the quantum amplitude estimation method. We use

the iterative quantum amplitude estimation [27]. In this method, repeated measurements are efficiently used to reduce the number of applications of the Grover oracle that amplifies the quantum amplitudes. The Grover oracle contains one normal and one inverse operation that encodes and decodes the quantum amplitude of interest. This operation is depicted in Fig. 5. The number of applications of the Grover oracle, N_{oracle} , can be bounded as

$$N_{\text{oracle}} \lesssim \frac{1.4}{\epsilon} \ln \left(\frac{2}{\delta} \log_2 \left(\frac{\pi}{4\epsilon} \right) \right), \quad (42)$$

where ϵ is the error tolerance and δ is the success probability [27].

In this cost estimation, we also have to take errors into account. In our algorithm, errors arise from the following sources.

- $\epsilon_{\text{estimation}}$ is errors in the quantum amplitude estimation,
- $\epsilon_{\text{calculation}}$ is errors in the probability calculation, including those caused by imperfect fixed-point arithmetic operations and the piecewise arcsin calculation,
- $\epsilon_{\text{rotation}}$ is errors in the controlled rotation operations, and
- ϵ_c is errors in the probability calculation.

The total error ϵ is constrained by the cumulative effects of these errors, scaled by the number of times each operation is performed. Therefore, the upper bound of the total error can be calculated as

$$\epsilon_{\text{max}} = 2N_{\text{oracle}}MH (\epsilon_{\text{calculation}} + \epsilon_{\text{rotation}}) + 2N_{\text{oracle}}\epsilon_c + \epsilon_{\text{estimation}}. \quad (43)$$

Table I lists the parameters of our resource estimation. Five different cases are considered, with differences in the number of bins N , the number of time steps M , and the maximum error ϵ_{max} . The parameters $n_\epsilon, d_\epsilon, M_\epsilon$ are related to $\epsilon_{\text{calculation}}$, and thus $\epsilon_{\text{calculation}}$ is chosen carefully to ensure that errors are sufficiently small.

The estimated quantum resources, including the number of logical qubits and T gates, are summarized in Table II. The estimation is for the calculation of the expected value of the number of droplets in the first bin of the final quantum state.

It shows that the required number of logical qubits ranges from 10^4 to 10^5 , while the number of T gates is on the order of 10^{14} to 10^{16} . The number of T gates increases by approximately a factor of 170 for every tenfold increase in N . When the number of time steps M increases or the maximum error ϵ_{max} decreases by a factor of 10, the number of T gates grows approximately tenfold in both cases. Notably, the number of logical qubits behaves differently: it increases by approximately a factor of 10 for a tenfold increase in M , but increases

by at most a factor of 2 or remains constant for a tenfold increase in N or ϵ_{\max} .

To identify which components dominate the overall cost, we separately analyze the T gate count and the logical qubit count. Our quantum circuit is built from a hierarchy of nested subroutines; for T gates, we quantify each component’s contribution by counting how many times each child subroutine is invoked by its parent. For logical qubits, we decompose the total into the number of qubits allocated to each register role. Both analyses are presented as stacked bar charts in Fig. 6 and Fig. 7, respectively. For T gates, the cost contributions are approximately even across all components in the baseline case (No. 1). As shown by comparing No. 1–3, growth in the total number of transition labels becomes the dominant factor as the number of bins N increases. Comparing No. 1 and No. 4, an increase in the number of time steps M makes the time-step contribution dominant. Comparing No. 1 and No. 5, reducing the maximum error makes the amplitude estimation contribution dominant. In contrast, for logical qubits, the primary cost contribution comes from the transition history qubits, whose number is proportional to the number of time steps M .

TABLE I. Parameters used in the estimation of quantum resources. N is the number of bins, M is the number of time steps, n_ϵ is the number of qubits for the piecewise arcsine calculation, d_ϵ and M_ϵ are the parameters for the piecewise arcsine calculation, $\epsilon_{\text{rotation}}$ is the error in the controlled rotation operations, $\epsilon_{\text{estimation}}$ is the error in the quantum amplitude estimation, and ϵ_c is the error in the probability calculation. In addition, $\delta = 0.01$ is used for the success probability in the quantum amplitude estimation for all cases.

case	N	M	n_ϵ	d_ϵ	M_ϵ	$\epsilon_{\text{rotation}}$	$\epsilon_{\text{estimation}}$	ϵ_c
No.1	40	2000	42	5	15	10^{-13}	9.9×10^{-3}	10^{-8}
No.2	126	2000	46	6	12	10^{-14}	9.9×10^{-3}	10^{-8}
No.3	400	2000	49	8	10	10^{-15}	9.9×10^{-3}	10^{-8}
No.4	40	20000	46	6	12	10^{-14}	9.9×10^{-3}	10^{-9}
No.5	40	2000	49	8	10	10^{-15}	9.9×10^{-4}	10^{-10}

TABLE II. Estimated quantum resources required for calculating the expected value of the number of droplets in the first bin. The resources include the maximum error ϵ_{\max} , the number of T gates (T-count), the T-depth, and the number of logical qubits. T-depth is the number of layers of T gates when gates that can be applied in parallel are grouped together.

case	ϵ_{\max}	T-count	T-depth	logical qubits
No.1	1.0×10^{-2}	4.9×10^{14}	3.5×10^{14}	1.9×10^4
No.2	1.0×10^{-2}	6.1×10^{15}	4.7×10^{15}	2.5×10^4
No.3	1.0×10^{-2}	8.2×10^{16}	6.5×10^{16}	3.4×10^4
No.4	1.0×10^{-2}	6.2×10^{15}	4.7×10^{15}	1.8×10^5
No.5	1.0×10^{-3}	8.7×10^{15}	6.9×10^{15}	1.9×10^4

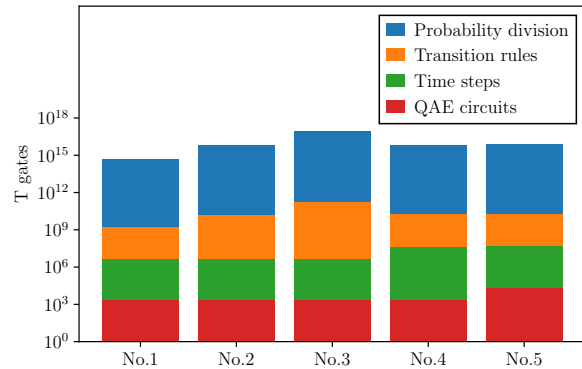


FIG. 6. Stacked bar charts showing how many times each child subroutine is invoked by its parent, decomposing the T gate count by component. “Probability division” refers to the number of T gates (T-count) for a single transition label of the probability division. “Transition rules” represent the number of the transition labels, corresponding to the number of individual probability divisions invoked within $U_{\Delta t}$. “Time steps” denote the number of $U_{\Delta t}$ operations executed within U_t . “Amplitude estimation” reflects the number of U_t operations invoked during a quantum amplitude estimation. The cost of the U_c operation is omitted as its contribution to the total cost is negligible.

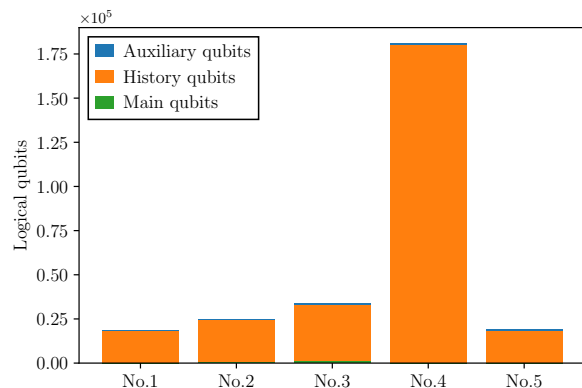


FIG. 7. The detailed breakdown of the number of logical qubits. “Auxiliary qubits” are used in the quantum circuit and the summation of the number of logical qubits $\mathcal{A}, \mathcal{B}, \mathcal{C}, \mathcal{D}$, and for quantum arithmetic. “History qubits” are the qubits used to encode the transition history. “Main qubits” are used to encode the droplet mass distribution. The numbers of auxiliary and main qubits are significantly smaller than the number of history qubits and barely visible in the figure.

V. DISCUSSION

In this collision-coalescence problem, the computational cost increases exponentially in classical calculations as the number of states grows [22]. For exam-

ple, if the computation for $N = 40$ requires one day, the same calculation for $N = 126$ would take 250 years, and for $N = 400$, it would take 5×10^{11} years, which is an impractical time frame. In contrast, quantum computing can limit the growth of T gate counts to approximately N^2 . This significant advantage arises from two key factors: the simultaneous execution of similar calculations enabled by the principle of superposition and the quadratic speedup achieved through the quantum amplitude estimation.

Furthermore, the representation of information is also improved. In our quantum algorithm, the qubits are separated into two parts to encode the system state and to encode the transition history, respectively. Additionally, the probability amplitudes are directly associated with the probabilities of the distributions. These approaches reduce the overhead of renormalization and allow avoiding unnecessary information loss. This structure facilitates the application of the quantum amplitude estimation in extracting information.

Although this study focuses on the time evolution of the probability distribution of cloud droplet sizes, our algorithm is potentially applicable to other problems that handle the time evolution of spectral probability distributions. For instance, our quantum algorithm may be useful in solving the probability distribution of turbulent kinetic energy spectra using a master equation with a collision kernel. Exploring such applications is an important direction for future research.

It would be useful to note the limitation of the proposed quantum algorithm. One major challenge is its high base computational cost. The number of T gates is typically kept up to 10^{14} in many quantum algorithms that are deemed promising, such as those for quantum chemistry [38–40]. While our algorithm significantly suppresses the growth in computational cost compared to classical methods, it still requires substantial resources for probability division and for handling time steps. Notably, this challenge is not unique to this study but is shared by the quantum finance areas [28]. Substantial progress is highly anticipated for these topics to make problems tractable.

To overcome this challenge, several strategies may be possible. One approach is to modify the problem settings to reduce computational demands. For instance, a piecewise approach could be employed to limit the number of time steps, rather than solving the system continuously across all time steps.

Another strategy is to utilize size-based distribution functions, as in spectral bin methods, to constrain the number of bins. These strategies render potential future research directions, aiming at reducing the computational cost of the quantum algorithm.

Despite this limitation, our results suggest that quantum computing has significant, yet still latent, potential to solve problems in atmospheric science, particularly in the cases where quantities of interest are expectations over probability distributions. This study demonstrated

its potential only on the computation of the expected values at the final time, but it also allows for extracting characteristic features from the time-series data since the calculated quantum states preserves all temporal information. Such analysis would be explored in future work.

VI. CONCLUSION

We have developed a quantum algorithm to simulate the collision-coalescence process of cloud droplets. The computation is based on the master equation that governs the time evolution of the probability distribution of droplet masses. By encoding this probability distribution into the quantum amplitudes, the algorithm can represent exponentially large state spaces efficiently in terms of qubit cost.

Unlike the conventional approaches, which explicitly encode the full distribution (e.g., mass distributions) at each time step, our method encodes only the history of transition events. This allows us to avoid storing all intermediate distributions, and to significantly reduce the number of qubits required for representing the time evolution. The time evolution is performed via the probability divisions, which can be executed in parallel for the identical transition labels. As a result, the computational cost scales only with the number of distinct transition labels. We have constructed the quantum circuit for the probability divisions using the quantum arithmetic operations and the controlled phase gates.

The algorithm is designed to estimate the expected number of droplets in each mass bin at the final time. Instead of measuring the full quantum state, the quantum amplitude estimation is used to directly estimate the amplitudes corresponding to the expected values. This reduces the number of repetitions required for readout.

We have estimated the quantum resources of the new algorithm by analyzing the number of the logical qubits and the T gates. The number of T gates scales as $\mathcal{O}(N^2)$, which is significantly smaller than the exponential cost of the classical simulations. However, the computational cost becomes high if the number of time steps increases. This point should be addressed in future work.

Our results demonstrate that the quantum computing has a potential to significantly reduce the computational cost of the simulation of the collision-coalescence process of cloud droplets. Thus, we conclude that the collision-coalescence process is one of the promising targets of the quantum computing in atmospheric science.

ACKNOWLEDGMENTS

We acknowledge for helpful discussions with Prof. Shinichiro Shima, Dr. Keita Kanno, and Dr. Yasunori Lee. This work was supported by JST SPRING, Grant Number JPMJSP2108 and International Graduate Program for Excellence in Earth-Space Science

(IGPEES), a World-leading Innovative Graduate Study (WINGS) Program, the University of Tokyo.

Appendix A: Fixed point quantum arithmetic operations

The fixed-point quantum arithmetic operations are used to calculate the transition probabilities. In this section, we explain the costs of implementing the fixed-point quantum arithmetic operations.

In our calculations, all values are positive. Also, as we show later, the values are either real number in the range of $[0, \pi/2]$ or integer. The real values are represented by the fixed-point numbers with the precision of n bits as

$$\alpha = \alpha_{n-1}2^0 + \alpha_{n-2}2^{-1} + \dots + \alpha_02^{-n+1}, \quad (\text{A1})$$

where $\alpha_i \in \{0, 1\}$ for each i and we can rewrite α as $\alpha_{n-1}.\alpha_{n-2}\dots\alpha_0$ in the binary representation. The integer values are represented as

$$\alpha = \alpha_{n-1}2^{n-1} + \alpha_{n-2}2^{n-2} + \dots + \alpha_02^0, \quad (\text{A2})$$

and $\alpha_{n-1}\alpha_{n-2}\dots\alpha_0$ in the binary representation.

Most of the calculations used in our algorithm follow the way used in [28], and this is summarized in their Appendix. We summarize the results of their resource estimation for these calculations in Table III. In addition, we explain briefly the operation that is different from the one in [28] in the following.

1. Comparison

The comparison operation is expressed as

$$\text{COMP}_n : |\alpha\rangle|\beta\rangle|0\rangle \rightarrow \begin{cases} |\alpha\rangle|\beta\rangle|1\rangle & \text{if } \alpha \geq \beta, \\ |\alpha\rangle|\beta\rangle|0\rangle & \text{otherwise.} \end{cases} \quad (\text{A3})$$

This operation is part of the COMP_CONST operation in [28]. The resulting circuit has

$$\begin{aligned} T_{\text{count}}(\text{COMP}_n) &= T_{\text{count}}(\text{SUB}_n) + T_{\text{count}}(\text{ADD}_n) \\ &= 8n - 16 \end{aligned} \quad (\text{A4})$$

T gates. T-depth is $4n - 8$ and the number of auxiliary qubits is $2n - 1$.

2. Multiplication

The fixed-point numbers we used here are expressed as either Eq. (A1) or Eq. (A2). As we show later, we only use the multiplication whose result is either an integer or lies between 0 and 1. We use standard shift-and-add strategy, which is also used in [28]. The multiplication between two integers α and β is expressed as

$$\text{MUL_INT}_{n,m} : |\alpha\rangle|\beta\rangle|0\rangle \rightarrow |\alpha\rangle|\beta\rangle|\alpha\beta\rangle, \quad (\text{A5})$$

where n and m are the number of bits of α and β , respectively, and $n \leq m$. The required T gates is

$$\begin{aligned} T_{\text{count}}(\text{MUL_INT}_{n,m}) &= \sum_{i=0}^{n-1} T_{\text{count}}(\text{c-ADD}_{m-i}) \\ &= \sum_{i=0}^{n-1} (8(m-i) - 4) \\ &= 8nm - 4n^2, \end{aligned} \quad (\text{A6})$$

T-depth is $4nm - 2n^2$ and the number of auxiliary qubits is $2n - 1$.

We also use the multiplication between two real numbers α and β who are in the range of $[0, 1]$ and whose bit length is both n . This operation is expressed as

$$\text{MUL_UI}_n : |\alpha\rangle|\beta\rangle|0\rangle \rightarrow |\alpha\rangle|\beta\rangle|\overline{\alpha\beta}\rangle, \quad (\text{A7})$$

where $\overline{\alpha\beta}$ is the n bit fixed-point representation of $\alpha\beta$. Here and throughout, \bar{x} denotes the n -bit fixed-point representation of a real number x . The required T gates is

$$\begin{aligned} T_{\text{count}}(\text{MUL_UI}_n) &= \sum_{i=0}^{n-1} T_{\text{count}}(\text{c-ADD}_{n-i}) \\ &= \sum_{i=0}^{n-1} (8(n-i) - 4) \\ &= 4n^2, \end{aligned} \quad (\text{A8})$$

T-depth is $2n^2$ and the number of auxiliary qubits is $2n - 1$.

When calculating the multiplication between an integer and a constant real number, we use the operation

$$\text{MUL_CONST_INT_UI}_{n,m} : |\alpha\rangle|0\rangle \rightarrow |\alpha\rangle|\overline{\alpha\beta}\rangle, \quad (\text{A9})$$

where n is the number of bits of the integer and m is the number of bits of the constant real number. The required T gates is

$$\begin{aligned} T_{\text{count}}(\text{MUL_CONST_INT_UI}_{n,m}) &= (m-n)T_{\text{count}}(\text{ADD}_n) + \sum_{i=0}^{n-1} T_{\text{count}}(\text{ADD}_{n-i}) \\ &= (m-n)(4n-4) + \sum_{i=0}^{m-1} (4(n-i) - 4) \\ &= 8nm - 4n^2 - 2m^2 - 4n - 6m. \end{aligned} \quad (\text{A10})$$

T-depth is $2nm - 2n^2 - m^2 - 2n - 3m$ and the number of auxiliary qubits is $n - 1$.

3. Square Root of real number between 0 and 1

The square root is described in [28], but we modified the operation to be suitable for our calculations with decimals. The square root of the fixed-point number α is

calculated as

$$\text{SQRT}_n : |\alpha\rangle |0\rangle \rightarrow |\alpha\rangle |\sqrt{\alpha}\rangle. \quad (\text{A11})$$

In our algorithm, $\alpha \in [0, 1]$. [28] gives the operation that number of digits in the result is halved. We modified this so that the operation is conducted until the last bit is reached. The resulting circuit has

$$\begin{aligned} T_{\text{count}}(\text{SQRT}_n) &= 2 \sum_{i=1}^{n-1} T_{\text{count}}(\text{ADD}_{2i}) + 2T_{\text{count}}(\text{c-ADD}_{2(n-1)}) \\ &= 2 \sum_{i=1}^{n-1} (8i - 4) + 2(16(n-1) - 4) \\ &= 8n^2 + 16n - 32 \end{aligned} \quad (\text{A12})$$

T gates. T-depth is $4n^2 + 8n - 16$ and the number of auxiliary qubits is $6n$.

4. Division of real number between 0 and 1.

The quantum division is expressed as

$$\text{DIV}_n : |\alpha\rangle |\beta\rangle |0\rangle \rightarrow |\alpha\rangle |\beta\rangle |\alpha/\beta\rangle. \quad (\text{A13})$$

In our algorithm, $\alpha, \beta, \alpha/\beta \in [0, 1]$. [41] proposed the so-called "long division" algorithm. This is an algorithm for integer division, but we can apply it to the division of real numbers between 0 and 1 and change it to calculate until the last bit is reached. Also, by using the do-copy-undo trick, we change it to the clean version described as Eq. (A13). The resulting circuit has

$$\begin{aligned} T_{\text{count}}(\text{DIV}_n) &= 2 \sum_{i=0}^{n-1} [T_{\text{count}}(\text{COMP}_{n-i}) + 2T_{\text{count}}(\text{c-SUB}_{n-i})] \\ &= 2 \sum_{i=0}^{n-1} [2(n-i) - 16 + 2(8(n-i) - 4)] \\ &= 18n^2 - 30n \end{aligned} \quad (\text{A14})$$

T gates. T-depth is $9n^2 - 15n$ and the number of auxiliary qubits is $2n - 1$.

5. Arcsine

The calculation of the arcsine is approximated by the piecewise polynomial function. This is expressed as

$$\text{ARCSIN}_{n,\epsilon} : |\alpha\rangle |0\rangle \rightarrow |\alpha\rangle |\overline{\text{pp}_{\text{arcsin}}(\alpha)}\rangle. \quad (\text{A15})$$

In our algorithm, $\alpha \in [0, 0.5]$ and $\overline{\text{pp}_{\text{arcsin}}(\alpha)} \in [0, 1]$. We apply the piecewise polynomial function described in [28]

to the arcsine calculation and our operation corresponds to $p = 1$ case. The resulting circuit has

$$\begin{aligned} T_{\text{count}}(\text{ARCSIN}_{n,\epsilon}) &= 4M_\epsilon T_{\text{count}}(\text{COMP_CONST}_n) \\ &+ 2d_\epsilon [T_{\text{count}}(\text{MUL_UI}_n) + T_{\text{count}}(\text{ADD}_n)] \\ &+ 4d_\epsilon M_\epsilon T_{\text{count}}(\text{Toffoli}_{\lceil \log_2(M_\epsilon) \rceil + 1}) \\ &= 4M_\epsilon(8n - 16) + 2d_\epsilon(4n^2 + 4n - 4) \\ &+ 16d_\epsilon M_\epsilon(\lceil \log_2(M_\epsilon) \rceil - 1) \end{aligned} \quad (\text{A16})$$

T gates. M_ϵ and d_ϵ are the number of pieces and the degree of the polynomial function corresponding to the precision ϵ , respectively. T-depth is $4d_\epsilon \max(2n^2, M_\epsilon(\lceil \log_2(M_\epsilon) \rceil - 1)) + 16M_\epsilon(n-2) + 4d_\epsilon(n-1)$ and the number of auxiliary qubits is $(d_\epsilon + 4)n + 2\lceil \log_2(M_\epsilon) \rceil$.

In order to determine M_ϵ and d_ϵ for given ϵ , we take a strategy of finding the minimum M_ϵ for given d_ϵ . Let $\Omega = [0, 0.5]$. We conduct the following steps to determine the minimum M_ϵ :

1. Set $\Omega_1 = [0, 0.5]$. Calculate the chebishev polynomial of degree d_ϵ that approximates the arcsin function on Ω_1 .
2. Calculate the L_∞ -error of the chebishev polynomial on Ω_1 .
3. If the error is less than ϵ , the minimum M_ϵ is 1. If not, set $\Omega_1 = [0, (0 + 0.5)/2]$.
4. Repeat the steps 1-3 until the error is less than ϵ , and determine the first subdomain $\Omega_1 = [0, a_1]$ that satisfies the condition.
5. Set $\Omega_2 = [a_1, 0.5]$ and repeat the steps 1-4 to determine the second subdomain $\Omega_2 = [a_2, a_3]$.
6. By repeating the steps 1-5 until a_i reaches 0.5, the minimum M_ϵ can be determined.

The result of this calculation is summarized in Table IV. In our actual calculations, we choose d_ϵ and M_ϵ that minimize the number of T gates from this table.

Appendix B: Quantum algorithm for operators U_P , U_{sin} , U_Q , U_{add} , U_R , U_{shift} , and U_c

1. Quantum algorithm for U_P

We utilize fixed-point quantum arithmetic operations to calculate transition probabilities. The operations are summarized in the Appendix of [28].

As written in Eq. (16), the U_P calculates the pieewise arcsin of the square root of a modified transition probability. The quantum circuit for U_P composed of the following operations:

TABLE III. The number of T gates and auxiliary qubits required for each fixed-point quantum arithmetic operation used in our cost estimation.

Operation	T-count	T-depth	auxiliary qubits	Techniques
Toffoli _n	4n - 8	n - 2	n - 1	[28], [42]
ADD _n	4n - 4	2n - 2	n - 1	[28], [43]
SUB _n	4n - 4	2n - 2	n - 1	[28], [43]
c-ADD _n	8n - 4	4n - 2	2n - 1	[28], [43]
c-SUB _n	8n - 4	4n - 2	2n - 1	[28], [43]
ADD_CONST _n	4n - 8	2n - 4	2n - 2	[28], [43]
COMP _n	8n - 16	4n - 8	2n - 1	[28], [43]
MUL_INT _{n,m}	8nm - 4n ²	4nm - 2n ²	2n - 1	[28], [43]
MUL_UI _n	4n ²	2n ²	2n - 1	[28], [43]
MUL_CONST_INT_UI _{n,m}	8nm - 4n ² - 2m ² -4n - 6m	2nm - 2n ² - m ² -2n - 3m	n - 1	[28], [43]
SQRT _n	8n ² + 16n - 32	4n ² + 8n - 16	6n	[28], [43], [44]
DIV _n	18n ² - 30n	9n ² - 15n	2n - 1	[41]
ARCSIN _{n,ε}	32M _ε (n - 2)	4d _ε max(2n ² , M _ε)	(d _ε + 4)n	[36], [28],
	+8d _ε (n ² + n - 1)	(⌈log ₂ (M _ε)⌉ - 1)		[42], [43],
	+16d _ε M _ε	+16M _ε (n - 2)		[45]
	(⌈log ₂ (M _ε)⌉ - 1)	+4d(n - 1)		

TABLE IV. The minimum M_ε and d_ε for given ε in the piecewise arcsine calculation.

ε	d _ε	M _ε
10 ⁻¹²	4	43
	5	15
	6	9
10 ⁻¹³	5	25
	6	12
	7	7
10 ⁻¹⁴	5	35
	6	18
	7	10
10 ⁻¹⁵	8	7
	6	27
	7	13
	8	10
	9	11

- Copy the number of droplets in the $i(h)$ -th and $j(h)$ -th bins to auxiliary qubits \mathcal{C}_1 and \mathcal{C}_2 :

$$|n_{i(h)}\rangle_{\mathcal{N}_{i(h)}} |n_{j(h)}\rangle_{\mathcal{N}_{j(h)}} |0\rangle_{\mathcal{C}_1} |0\rangle_{\mathcal{C}_2} \rightarrow |n_{i(h)}\rangle_{\mathcal{N}_{i(h)}} |n_{j(h)}\rangle_{\mathcal{N}_{j(h)}} |n_{i(h)}\rangle_{\mathcal{C}_1} |n_{j(h)}\rangle_{\mathcal{C}_2}. \quad (\text{B1})$$

\mathcal{C}_1 and \mathcal{C}_2 are both q_1 qubits. In this step, CNOT gates are only used.

- Compute multiplication of $n_{i(h)}$ and $n_{j(h)}$ and store the result in auxiliary qubits \mathcal{C}_3 :

$$|n_{i(h)}\rangle_{\mathcal{C}_1} |n_{j(h)}\rangle_{\mathcal{C}_2} |0\rangle_{\mathcal{C}_3} \rightarrow |n_{i(h)}\rangle_{\mathcal{C}_1} |n_{j(h)}\rangle_{\mathcal{C}_2} |n_{i(h)}n_{j(h)}\rangle_{\mathcal{C}_3}. \quad (\text{B2})$$

\mathcal{C}_3 is $2q_1$ qubits. In this step, MUL_INT _{q_1, q_1} is used.

- Compute the multiplication of $n_{i(h)}n_{j(h)}$ and $K(i(h), j(h))\Delta t$ and store the result $r_h = n_{i(h)}n_{j(h)}K(i(h), j(h))\Delta t$ in auxiliary qubits \mathcal{C}_4 :

$$|n_{i(h)}n_{j(h)}\rangle_{\mathcal{C}_3} |0\rangle_{\mathcal{C}_4} \rightarrow |n_{i(h)}n_{j(h)}\rangle_{\mathcal{C}_3} |r_h\rangle_{\mathcal{C}_4}. \quad (\text{B3})$$

\mathcal{C}_4 is n_ϵ qubits, where n_ϵ is the number of bits to express the transition probability. In this step, MUL_CONST_INT_UI _{$2q_1, n_\epsilon$} is used.

- Compare r_h and $s_{h+1}/4$ and store the result in auxiliary qubits \mathcal{C}_5 :

$$|s_{h+1}\rangle_{\mathcal{A}} |r_h\rangle_{\mathcal{C}_4} |0\rangle_{\mathcal{C}_5} \rightarrow |s_{h+1}\rangle_{\mathcal{A}} |r_h\rangle_{\mathcal{C}_4} |z\rangle_{\mathcal{C}_5}, \quad (\text{B4})$$

where $z = 1$ if $r_h \geq s_{h+1}/4$ and $z = 0$ otherwise. \mathcal{C}_5 is 1 qubit. In this step, COMP _{n_ϵ} is used. This step is needed to guarantee that the input to the arcsin function, which is used in the step 8 does not exceed $1/4$.

- Based on the result of the comparison, store $|w\rangle$ in auxiliary qubits \mathcal{C}_6 :

$$|z\rangle_{\mathcal{C}_5} |0\rangle_{\mathcal{C}_6} \rightarrow |z\rangle_{\mathcal{C}_5} |w\rangle_{\mathcal{C}_6}, \quad (\text{B5})$$

where $w = s_{h+1} - r_h$ if $z = 1$ and $w = r_h$ otherwise. \mathcal{C}_6 is n_ϵ qubits. In this step, c-SUB _{n_ϵ} is used.

- Compute the square root of w and store the result in auxiliary qubits \mathcal{C}_7 :

$$|w\rangle_{\mathcal{C}_6} |0\rangle_{\mathcal{C}_7} \rightarrow |w\rangle_{\mathcal{C}_6} |\sqrt{w}\rangle_{\mathcal{C}_7}. \quad (\text{B6})$$

\mathcal{C}_7 is n_ϵ qubits. In this step, SQRT _{n_ϵ} is used.

- Compute the square root of s_{h+1} and store the result in auxiliary qubits \mathcal{C}_8 :

$$|s_{h+1}\rangle_{\mathcal{A}} |0\rangle_{\mathcal{C}_8} \rightarrow |s_{h+1}\rangle_{\mathcal{A}} |\sqrt{s_{h+1}}\rangle_{\mathcal{C}_8}. \quad (\text{B7})$$

\mathcal{C}_8 is n_ϵ qubits. In this step, SQRT _{n_ϵ} is used.

8. Compute the division of \sqrt{w} and $\sqrt{s_{h+1}}$ and store the result in auxiliary qubits \mathcal{C}_9 :

$$|\sqrt{w}\rangle_{\mathcal{C}_7} |\sqrt{s_{h+1}}\rangle_{\mathcal{C}_8} |0\rangle_{\mathcal{C}_9} \rightarrow |\sqrt{w}\rangle_{\mathcal{C}_7} |\sqrt{s_{h+1}}\rangle_{\mathcal{C}_8} |\sqrt{w/s_{h+1}}\rangle_{\mathcal{C}_9}. \quad (\text{B8})$$

\mathcal{C}_9 is n_ϵ qubits. In this step, DIV_{n_ϵ} is used.

9. Compute the pieewise arcsin of $\sqrt{w/s_{h+1}}$ and store the result in auxiliary qubits \mathcal{B} :

$$|0\rangle_{\mathcal{B}} |\sqrt{w/s_{h+1}}\rangle_{\mathcal{C}_9} \rightarrow |\text{pp}_{\arcsin} \sqrt{w/s_{h+1}}\rangle_{\mathcal{B}} |\sqrt{w/s_{h+1}}\rangle_{\mathcal{C}_9}. \quad (\text{B9})$$

In this step, $\text{ARCSIN}_{n_\epsilon, \epsilon_{\arcsin}}$ is used.

10. Finally, set the state of the auxiliary qubits \mathcal{B} to $|\pi/2 - \text{pp}_{\arcsin} \sqrt{w/s_{h+1}}\rangle$ if $z = 1$ and $|\text{pp}_{\arcsin} \sqrt{w/s_{h+1}}\rangle$ otherwise, which corresponds to the arcsin $\sqrt{r'_h}$:

$$|\text{pp}_{\arcsin} \sqrt{w/s_{h+1}}\rangle_{\mathcal{B}} |z\rangle_{\mathcal{C}_5} \rightarrow |\text{pp}_{\arcsin} \sqrt{r'_h}\rangle_{\mathcal{B}} |z\rangle_{\mathcal{C}_5}. \quad (\text{B10})$$

In this step, $\text{c-SUB}_{n_\epsilon}$ and CNOT gates are used.

In total, the U_P gate requires 1 $\text{MUL_INT}_{q_1, q_1}$, 1 $\text{MUL_CONST_INT_UI}_{2q_1, n_\epsilon}$, 1 COMP_{n_ϵ} , 2 $\text{c-SUB}_{n_\epsilon}$, 2 SQRT_{n_ϵ} , 1 DIV_{n_ϵ} , and 1 $\text{ARCSIN}_{n_\epsilon, \epsilon_{\arcsin}}$. The number of T gates required for each operation is summarized in the Table III. The U_P gate requires \mathcal{C}_1 to \mathcal{C}_9 auxiliary qubits and also requires additional auxiliary qubits to perform the quantum arithmetic operations. The number of auxiliary qubits required for each operation is summarized in the Table III.

2. Quantum algorithm for U_{\sin}

By using \mathcal{B} as a control qubit, the U_{\sin} gate reflect the transition probability into the quantum amplitude when the transition history state is 0. We slightly modify the method introduced in the Appendix B of [28] in order to operate U_{\sin} only when the transition history state is 0. What we want to do is that

$$\begin{aligned} & |0\rangle_{\mathcal{H}_m[q_h-1:1]} |0\rangle_{\mathcal{H}_m[0]} |\text{pp}_{\arcsin} \sqrt{r'_h}\rangle_{\mathcal{B}} \\ & \rightarrow |0\rangle_{\mathcal{H}_m[q_h-1:1]} \left(\sqrt{1-r'_h} |0\rangle_{\mathcal{H}_m[0]} + \sqrt{r'_h} |1\rangle_{\mathcal{H}_m[0]} \right) \\ & \quad |\text{pp}_{\arcsin} \sqrt{r'_h}\rangle_{\mathcal{B}}. \quad (\text{B11}) \end{aligned}$$

When we write as

$$\text{pp}_{\arcsin} \sqrt{r'_h} = \alpha_{n-1} + \alpha_{n-2} 2^{-1} + \dots + \alpha_0 2^{1-n}, \quad (\text{B12})$$

Eq. (B11) can be implemented using the quantum circuit depicted in Fig. 8. It is possible because the quantum state $|h\rangle_{\mathcal{H}_m}$ satisfies either $h \geq 2$ or $h = 0$.

The multicontrolled $R_y(\theta)$ gates are compiled using [46] as described in Fig. 9. This circuit has 6 R_z gates

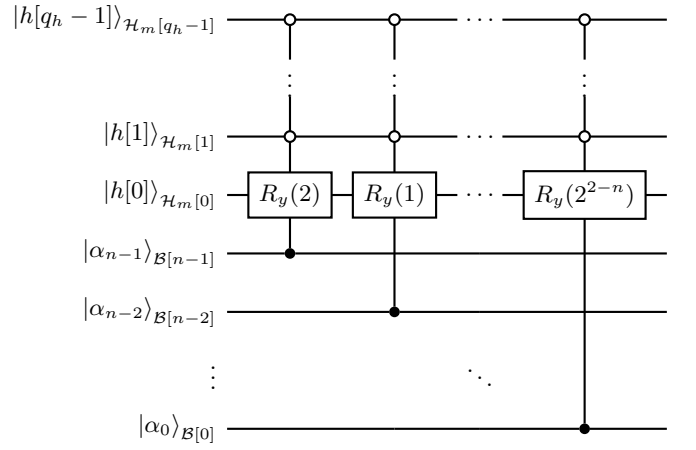


FIG. 8. The quantum circuit for U_{\sin} .

and 6 R_z depth. We can reduce the R_z depth by utilizing the same technique as in [28]. The depth reduced circuit is depicted in Fig. 10. Also, by utilizing the relationship depicted in Fig. 11, we obtain the circuit corresponding to the multicontrolled $R_y(\theta)$ gate as depicted in Fig. 12.

The area enclosed by the dashed line in Fig. 12 can be implemented effectively by utilizing the recursive phase catalysis circuit described in [28]. The total cost required for U_{\sin} is:

$$T_{\text{count}}(U_{\sin}) = 12n_\epsilon + 6.6 \log_2(4/\epsilon_{\sin}) + 8q_h - 16, \quad (\text{B13})$$

$$T_{\text{depth}}(U_{\sin}) = 3n_\epsilon + 1.15 \log_2(4/\epsilon_{\sin}) + 2q_h - 3, \quad (\text{B14})$$

$$a_{\text{count}}(U_{\sin}) = 5n_\epsilon + 2, \quad (\text{B15})$$

where n_ϵ is the number of qubits of \mathcal{B} and ϵ_{\sin} is the error tolerance for this operation.

3. Quantum algorithm for U_Q

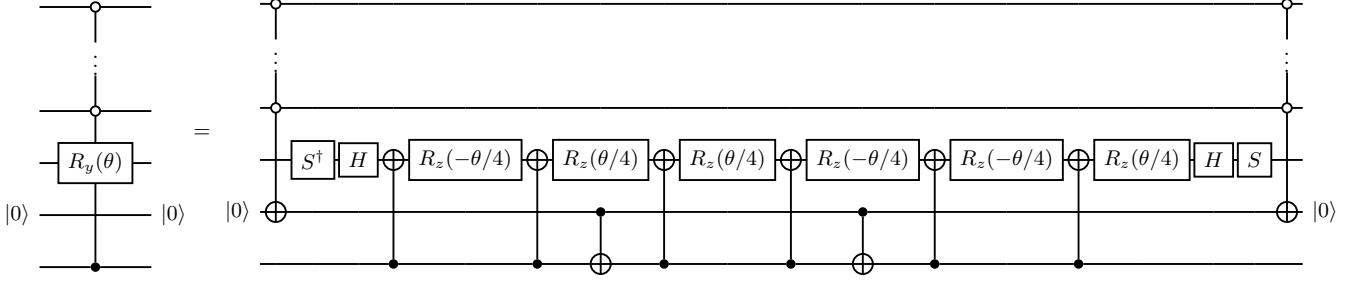
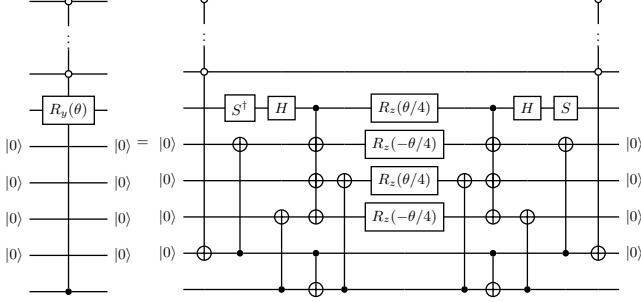
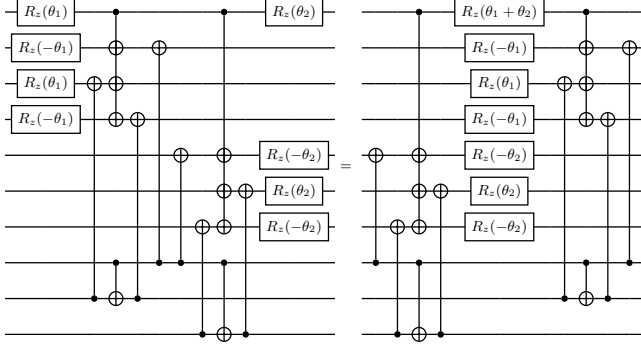
The U_Q gate uncomputes the auxiliary states stored in the qubits \mathcal{B} and \mathcal{C} while updating s_{h+1} to s_h . The quantum circuit for U_Q composed of the following operations:

1. Conduct inverse operation of step 10 to 4 in U_P gate and uncompute the auxiliary qubits $\mathcal{B}, \mathcal{C}_5$ to \mathcal{C}_9 :

$$\begin{aligned} & |s_{h+1}\rangle_{\mathcal{A}} |\text{pp}_{\arcsin} \sqrt{r'_h}\rangle_{\mathcal{B}} |r_h\rangle_{\mathcal{C}_4} |z\rangle_{\mathcal{C}_5} |w\rangle_{\mathcal{C}_6} \\ & \quad |\sqrt{w}\rangle_{\mathcal{C}_7} |\sqrt{s_{h+1}}\rangle_{\mathcal{C}_8} |\sqrt{w/s_{h+1}}\rangle_{\mathcal{C}_9} \\ & \rightarrow |s_{h+1}\rangle_{\mathcal{A}} |0\rangle_{\mathcal{B}} |r_h\rangle_{\mathcal{C}_4} |0\rangle_{\mathcal{C}_5} |0\rangle_{\mathcal{C}_6} |0\rangle_{\mathcal{C}_7} |0\rangle_{\mathcal{C}_8} |0\rangle_{\mathcal{C}_9}. \quad (\text{B16}) \end{aligned}$$

2. Compute the $s_h = s_{h+1} - r_h$ from r_h and s_{h+1} :

$$|s_{h+1}\rangle_{\mathcal{A}} |r_h\rangle_{\mathcal{C}_4} \rightarrow |s_h\rangle_{\mathcal{A}} |r_h\rangle_{\mathcal{C}_4}. \quad (\text{B17})$$

FIG. 9. The quantum circuit for multicontrolled $R_y(\theta)$ gate.FIG. 10. The quantum circuit for multicontrolled $R_y(\theta)$ gate with reduced depth.FIG. 11. The relationship between the multicontrolled R_z gates.

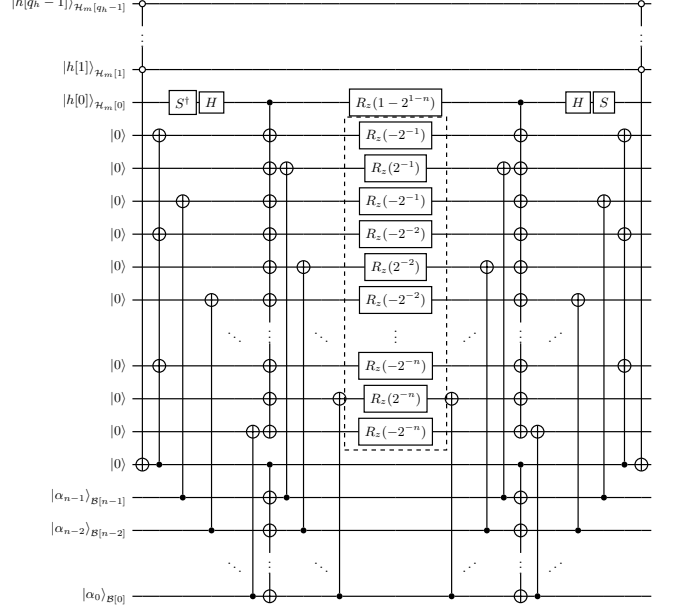
3. Conduct inverse operation of step 3, 2, and 1 in U_P gate and uncompute the auxiliary qubits \mathcal{C}_1 to \mathcal{C}_4 :

$$\begin{aligned} & |n_i(h)\rangle_{\mathcal{N}_i(h)} |n_j(h)\rangle_{\mathcal{N}_j(h)} |n_i(h)\rangle_{\mathcal{C}_1} |n_j(h)\rangle_{\mathcal{C}_2} |n_i(h)n_j(h)\rangle_{\mathcal{C}_3} |r_h\rangle_{\mathcal{C}_4} \\ & \rightarrow |n_i(h)\rangle_{\mathcal{N}_i(h)} |n_j(h)\rangle_{\mathcal{N}_j(h)} |0\rangle_{\mathcal{C}_1} |0\rangle_{\mathcal{C}_2} |0\rangle_{\mathcal{C}_3} |0\rangle_{\mathcal{C}_4}. \end{aligned} \quad (\text{B18})$$

In total, the U_Q gate requires 1 MUL_INT $_{q_1, q_1}$, 1 MUL_CONST_INT_UI $_{2q_1, n_\epsilon}$, 1 COMP $_{n_\epsilon}$, 2 c-SUB $_{n_\epsilon}$, 2 SQRT $_{n_\epsilon}$, 1 DIV $_{n_\epsilon}$, 1 ARCSIN $_{n_\epsilon, \epsilon_{\text{arcsin}}}$, and 1 SUB $_{n_\epsilon}$.

4. Quantum algorithm for U_{add}

The U_{add} gate adds constant 1 to the transition history qubits when the transition state qubits are not $|0\rangle_{\mathcal{H}_m}$ and

FIG. 12. The quantum circuit for multicontrolled $R_y(\theta)$ gate.

does nothing when the transition state qubits are $|0\rangle_{\mathcal{H}_m}$. The quantum circuit for U_{add} composed of the following operations:

1. Add 1 to the history qubits \mathcal{H}_m :

$$\sum_{k=0}^{h-1} |k\rangle_{\mathcal{H}_m} \rightarrow \sum_{k=0}^{h-1} |k+1\rangle_{\mathcal{H}_m} = \sum_{k=1}^h |k\rangle_{\mathcal{H}_m}. \quad (\text{B19})$$

In this step, ADD_CONST $_{q_h}$ is used.

2. Apply CNOT gate to the least significant digit of the history qubits \mathcal{H}_m to restore to its original zero state:

$$\sum_{k=1}^h |k\rangle_{\mathcal{H}_m} \rightarrow |0\rangle_{\mathcal{H}_m} + \sum_{k=2}^h |k\rangle_{\mathcal{H}_m}. \quad (\text{B20})$$

In this step, Toffoli $_H$ is used.

In total, the U_{add} gate requires 1 ADD_CONST $_{q_h}$ and 1 Toffoli $_{q_h}$.

5. Quantum algorithm for U_R

The U_R gate uncomputes the auxiliary states stored in the qubits \mathcal{A} as

$$|s_h\rangle_{\mathcal{A}} \rightarrow |s_{h+1}\rangle_{\mathcal{A}}. \quad (\text{B21})$$

The quantum circuit for U_R composed of the inverse operation of step 2 and 3 of U_Q and the inverse operation of step 1 to 3 of U_P gate. The total cost required for U_R is 2 MUL_INT $_{q_1, q_1}$, 2 MUL_CONST_INT_UI $_{2q_1, n_\epsilon}$, and 1 ADD $_{n_\epsilon}$.

6. Quantum algorithm for U_{shift}

The U_{shift} gate shifts the mass distribution \bar{n} to \bar{n}' according to the transition rule h_m stored in the history qubits \mathcal{H}_m . The process is one of the following:

1. The number of droplets in the i -th and j -th bins decreases by one, and the number of droplets in the $i + j$ -th bin increases by one.
2. The number of droplets in the i -th bin decreases

by two, and the number of droplets in the $2i$ -th bin increases by one.

In either case, the shift can be realized by utilizing multi-controlled ADD (SUB) gate. The multicontrolled ADD (SUB) gate can be organized by utilizing Toffoli gate and c-ADD (c-SUB) gate. Therefore, the total cost required for the U_{shift} gate is 2 Toffoli $_{q_h}$, 1 c-ADD $_{q_i+j}$, 1 c-SUB $_{q_i}$, and 1 c-SUB $_{q_j}$ for the first case and 1 Toffoli $_{q_h}$, 1 c-ADD $_{q_{2i}}$, and 1 c-SUB $_{q_i}$ for the second case.

7. Quantum algorithm for U_c

The U_c gate are composed of repeating implementation of R_y gates. The number of repetition is determined by I for the i -th bin. The total cost required for U_c is

$$T_{\text{count}}(U_c) = 1.15I \log_2(I/\epsilon_c), \quad (\text{B22})$$

where ϵ_c is the error tolerance for this operation. We utilize the repeat until success method [47] to implement the R_y gates.

-
- [1] D. A. Randall, Editor and J. Zehnder, Reviewer, General circulation model development: Past, present, and future. international geophysics series, vol 70, *Appl. Mech. Rev.* **54**, B94 (2001).
- [2] M. Ghil and V. Lucarini, The physics of climate variability and climate change, *Rev. Mod. Phys.* **92**, 035002 (2020).
- [3] Intergovernmental Panel on Climate Change (IPCC), *Climate change 2021 – the physical science basis: Working group I contribution to the sixth assessment report of the intergovernmental panel on climate change* (Cambridge University Press, Cambridge, England, 2023).
- [4] Intergovernmental Panel on Climate Change (IPCC), *Climate change 2022 – impacts, adaptation and vulnerability: Working group II contribution to the sixth assessment report of the intergovernmental panel on climate change* (Cambridge University Press, Cambridge, England, 2023).
- [5] *Climate change 2022 - mitigation of climate change: Working group III contribution to the sixth assessment report of the intergovernmental panel on climate change* (2023).
- [6] W. S. Parker, Predicting weather and climate: Uncertainty, ensembles and probability, *Stud. Hist. Philos. Sci. B Stud. Hist. Philos. Modern Phys.* **41**, 263 (2010).
- [7] R. Mizuta, A. Murata, M. Ishii, H. Shiogama, K. Hibino, N. Mori, O. Arakawa, Y. Imada, K. Yoshida, T. Aoyagi, H. Kawase, M. Mori, Y. Okada, T. Shimura, T. Nagatomo, M. Ikeda, H. Endo, M. Nosaka, M. Arai, C. Takahashi, K. Tanaka, T. Takemi, Y. Tachikawa, K. Temur, Y. Kamae, M. Watanabe, H. Sasaki, A. Kitoh, I. Takayabu, E. Nakakita, and M. Kimoto, Over 5,000 years of ensemble future climate simulations by 60-km global and 20-km regional atmospheric models, *Bull. Am. Meteorol. Soc.* **98**, 1383 (2017).
- [8] G. Tegegne, A. M. Melesse, and A. W. Worqlul, Development of multi-model ensemble approach for enhanced assessment of impacts of climate change on climate extremes, *Sci. Total Environ.* **704**, 135357 (2020).
- [9] J. Berner, U. Achatz, L. Batté, L. Bengtsson, A. d. I. Cámara, H. M. Christensen, M. Colangeli, D. R. B. Coleman, D. Crommelin, S. I. Dolaptchiev, C. L. E. Franzke, P. Friederichs, P. Imkeller, H. Järvinen, S. Juricke, V. Kitsios, F. Lott, V. Lucarini, S. Mahajan, T. N. Palmer, C. Penland, M. Sakradzija, J.-S. von Storch, A. Weisheimer, M. Weniger, P. D. Williams, and J.-I. Yano, Stochastic parameterization: Toward a new view of weather and climate models, *Bull. Am. Meteorol. Soc.* **98**, 565 (2017).
- [10] W. W. Grabowski and P. K. Smolarkiewicz, CRCP: a cloud resolving convection parameterization for modeling the tropical convecting atmosphere, *Physica D* **133**, 171 (1999).
- [11] W. W. Grabowski, An improved framework for superparameterization, *J. Atmos. Sci.* **61**, 1940 (2004).
- [12] R. Buizza, M. Milleer, and T. N. Palmer, Stochastic representation of model uncertainties in the ECMWF ensemble prediction system, *Q. J. R. Meteorol. Soc.* **125**, 2887 (1999).
- [13] T. N. Palmer, R. Buizza, F. Doblas-Reyes, T. Jung, M. Leutbecher, G. J. Shutts, M. Steinheimer, and A. Weisheimer, *Stochastic parametrization and model uncertainty* (2009).
- [14] X. Qiao, S. Wang, and J. Min, A stochastic perturbed parameterization tendency scheme for diffusion (SPPTD) and its application to an idealized supercell simulation,

- Mon. Weather Rev.* **145**, 2119 (2017).
- [15] A. Khain, A. Pokrovsky, M. Pinsky, A. Seifert, and V. Phillips, Simulation of effects of atmospheric aerosols on deep turbulent convective clouds using a spectral microphysics mixed-phase cumulus cloud model. part I: Model description and possible applications, *J. Atmos. Sci.* **61**, 2963 (2004).
- [16] L.-P. Wang, Y. Xue, O. Ayala, and W. W. Grabowski, Effects of stochastic coalescence and air turbulence on the size distribution of cloud droplets, *Atmos. Res.* **82**, 416 (2006).
- [17] H. Morrison and W. W. Grabowski, An improved representation of rimed snow and conversion to graupel in a multicomponent bin microphysics scheme, *J. Atmos. Sci.* **67**, 1337 (2010).
- [18] W. W. Grabowski, H. Morrison, S.-I. Shima, G. C. Abade, P. Dziekan, and H. Pawlowska, Modeling of cloud microphysics: Can we do better?, *Bull. Am. Meteorol. Soc.* **100**, 655 (2019).
- [19] S. Shima, K. Kusano, A. Kawano, T. Sugiyama, and S. Kawahara, The super-droplet method for the numerical simulation of clouds and precipitation: a particle-based and probabilistic microphysics model coupled with a non-hydrostatic model, *Quarterly Journal of the Royal Meteorological Society* **135**, 1307 (2009).
- [20] S.-I. Shima, Y. Sato, A. Hashimoto, and R. Misumi, Predicting the morphology of ice particles in deep convection using the super-droplet method: development and evaluation of SCALE-SDM 0.2.5-2.2.0, -2.2.1, and -2.2.2, *Geosci. Model Dev.* **13**, 4107 (2020).
- [21] D. T. Gillespie, The stochastic coalescence model for cloud droplet growth, *J. Atmos. Sci.* **29**, 1496 (1972).
- [22] L. Alfonso, An algorithm for the numerical solution of the multivariate master equation for stochastic coalescence, *Atmos. Chem. Phys.* **15**, 12315 (2015).
- [23] D. P. Landau and K. Binder, *A guide to Monte Carlo simulations in statistical physics*, 4th ed. (Cambridge University Press, Cambridge, England, 2014).
- [24] P. Rebentrost, B. Gupt, and T. R. Bromley, Quantum computational finance: Monte carlo pricing of financial derivatives, *Phys. Rev. A* **98**, 022321 (2018).
- [25] D. Herman, C. Googin, X. Liu, Y. Sun, A. Galda, I. Safro, M. Pistoia, and Y. Alexeev, Quantum computing for finance, *Nat. Rev. Phys.* **5**, 450 (2023).
- [26] G. Brassard, P. Hoyer, M. Mosca, and A. Tapp, *Quantum amplitude amplification and estimation*, Book (2002).
- [27] D. Grinko, J. Gacon, C. Zoufal, and S. Woerner, Iterative quantum amplitude estimation, *Npj Quantum Inf.* **7**, 1 (2021).
- [28] G. Wang and A. Kan, Option pricing under stochastic volatility on a quantum computer, *Quantum* **8**, 1504 (2024).
- [29] R. R. Rogers and M. K. Yau, *A Short Course in Cloud Physics*, 3rd ed. (Butterworth-Heinemann, Oxford, England, 1996).
- [30] H. Morrison, M. van Lier-Walqui, A. M. Fridlind, W. W. Grabowski, J. Y. Harrington, C. Hoose, A. Korolev, M. R. Kumjian, J. A. Milbrandt, H. Pawlowska, D. J. Posselt, O. P. Prat, K. J. Reimel, S.-I. Shima, B. van Diedenoven, and L. Xue, Confronting the challenge of modeling cloud and precipitation microphysics, *J. Adv. Model. Earth Syst.* **12**, e2019MS001689 (2020).
- [31] A. P. Khain, K. D. Beheng, A. Heymsfield, A. Korolev, S. O. Krichak, Z. Levin, M. Pinsky, V. Phillips, T. Prabhakaran, A. Teller, S. C. van den Heever, and J.-I. Yano, Representation of microphysical processes in cloud-resolving models: Spectral (bin) microphysics versus bulk parameterization: BIN VS BULK, *Rev. Geophys.* **53**, 247 (2015).
- [32] P. Dziekan and H. Pawlowska, Stochastic coalescence in lagrangian cloud microphysics, *Atmos. Chem. Phys.* **17**, 13509 (2017).
- [33] H. Tanaka and K. Nakazawa, Stochastic coagulation equation and validity of the statistical coagulation equation, *J. Geomagn. Geoelectr.* **45**, 361 (1993).
- [34] M. Hall, *Combinatorial Theory*, 2nd ed., Wiley Classics Library (Wiley-Interscience, New York, 2011).
- [35] L. Alfonso and G. B. Raga, The impact of fluctuations and correlations in droplet growth by collision-coalescence revisited - part 1: Numerical calculation of post-gel droplet size distribution, *Atmos. Chem. Phys.* **17**, 6895 (2017).
- [36] T. Häner, M. Roetteler, and K. M. Svore, Optimizing quantum circuits for arithmetic, arXiv [quant-ph] (2018).
- [37] J. J. Goings, A. White, J. Lee, C. S. Tautermann, M. Degroote, C. Gidney, T. Shiozaki, R. Babbush, and N. C. Rubin, Reliably assessing the electronic structure of cytochrome P450 on today's classical computers and tomorrow's quantum computers, *Proc. Natl. Acad. Sci. U. S. A.* **119**, e2203533119 (2022).
- [38] V. von Burg, G. H. Low, T. Häner, D. S. Steiger, M. Reiher, M. Roetteler, and M. Troyer, Quantum computing enhanced computational catalysis, *Phys. Rev. Res.* **3**, 10.1103/physrevresearch.3.033055 (2021).
- [39] N. C. Rubin, D. W. Berry, F. D. Malone, A. F. White, T. Khattar, A. E. DePrince, S. Siculo, M. Kühn, M. Kaicher, J. Lee, and R. Babbush, Fault-tolerant quantum simulation of materials using bloch orbitals, *PRX quantum* **4**, 10.1103/prxquantum.4.040303 (2023).
- [40] J. Lee, D. W. Berry, C. Gidney, W. J. Huggins, J. R. McClean, N. Wiebe, and R. Babbush, Even more efficient quantum computations of chemistry through tensor hypercontraction, *PRX quantum* **2**, 10.1103/prxquantum.2.030305 (2021).
- [41] F. Orts, R. Paulavičius, and E. Filatovas, Quantum circuit optimization of an integer divider, *J. Syst. Softw.* **215**, 112091 (2024).
- [42] C. Jones, Low-overhead constructions for the fault-tolerant toffoli gate, *Phys. Rev. A* **87**, 022328 (2013).
- [43] C. Gidney, Halving the cost of quantum addition, *Quantum* **2**, 74 (2018).
- [44] E. Muñoz-Coreas and H. Thapliyal, T-count and qubit optimized quantum circuit design of the non-restoring square root algorithm, *ACM J. Emerg. Technol. Comput. Syst.* **14**, 1 (2018).
- [45] S. Chakrabarti, R. Krishnakumar, G. Mazzola, N. Stamatopoulos, S. Woerner, and W. J. Zeng, A threshold for quantum advantage in derivative pricing, *Quantum* **5**, 463 (2021).
- [46] M. A. Nielsen and I. L. Chuang, *Quantum Computation and Quantum Information* (Cambridge University Press, Cambridge, England, 2010).
- [47] A. Bocharov, M. Roetteler, and K. M. Svore, Efficient synthesis of universal repeat-until-success quantum circuits, *Phys. Rev. Lett.* **114**, 080502 (2015).